Engineered Science
DOI: https://dx.doi.org/10.30919/es1640

Advances in Electromagnetic Interference Shielding Materials with Low Reflection

Li Lang,[1] Weining Ren,[1] Jingyi Men,[1] Xinyuan Mao,[1] Zelong Yang,[1] Shengrui Zhang[1] and Lei Wang[1,2,*]

Abstract

With the rapid development of electronic information technology, electromagnetic radiation is ubiquitous in the environment, seriously interfering with the normal operation of other electronic components and human health. However, traditional metal-based electromagnetic interference (EMI) shielding materials usually cause high reflection, resulting in secondary environmental pollution. Therefore, the development of EMI shielding materials with low reflection coefficient (R) and high EMI shielding effectiveness (SE) has received extensive attention from scholars. In this review, the research progress and development trends of low-reflection EMI shielding materials are systematically expounded. Firstly, the shielding mechanism of low-reflection EMI shielding materials is briefly introduced. Then, the preparation methods and structural designs of low-reflection EMI shielding materials are reviewed in detail. Finally, the key scientific and technological problems of low-reflection EMI shielding materials are proposed, and the future development trends are prospected.

Keywords: Electromagnetic interference; Low reflection; Structural designs; EMI shielding composites.
Received: 29 May 2025; Revised: 27 June 2025; Accepted: 21 July 2025.
Article type: Review article.

1. Introduction

With the emergence of new-generation information technologies like 5G communication and the Internet of Things, electronic devices are evolving in the directions of higher frequencies, greater power, and higher integration.[1,2] The electromagnetic radiation produced during the operation of these devices not only interferes with the operation of other electronic components but also poses potential hazards to human health.[3,4] The utilization of electromagnetic interference (EMI) shielding materials to block electromagnetic waves (EMWs) is an effective approach to guarantee the normal operation of electronic devices and human health.[5,6] Nevertheless, conventional metal-based EMI shielding materials typically cause high reflection, which is prone to result in severe secondary pollution.[7-9] Hence, the development of EMI shielding materials with low reflection and high absorption characteristics to achieve "green shielding" has become a research focus and an important development trend in the fields of electromagnetic protection.[10-12]

Currently, the research on EMI shielding materials primarily focuses on achieving superior EMI shielding performance through enhancing electrical conductivity (σ).[13-15] However, high σ can lead to impedance mismatch between the service environment and shielding materials. As a result, most of the incident EMWs are reflected from the material surface into the free space with lower impedance, where they continue to propagate.[16-18] This not only complicates the electromagnetic environment but also causes secondary pollution. Therefore, addressing the trade-off between high EMI shielding effectiveness (SE) and low reflection coefficient (R) has emerged as a critical challenge and an important research topic.[19] In recent years, researchers have put forward an "absorption-dominated" EMI shielding mode, which realizes effective dissipation by converting the incident EMWs energy into heat energy and other forms rather than mere reflection.[20-22] To attain this objective, researchers have mainly concentrated on the following aspects: (1) Introducing magnetic components (such as Fe_3O_4, CoNi, *etc.*) to establish an electromagnetic synergetic loss network;[23,24] (2) Designing structures with gradient variations in σ/magnetic permeability to optimize impedance matching;[25,26] (3) Developing multi-layer heterogeneous interfaces and porous structures to enhance multiple scattering. These strategies, by regulating

[1] *School of Chemistry and Environment Science, Shaanxi University of Technology, Hanzhong, Shaanxi, 723001, China*
[2] *Shaanxi Key Laboratory of Macromolecular Science and Technology, School of Chemistry and Chemical Engineering, Northwestern Polytechnical University, Xi'an, Shaanxi, 710072, China*
**E-mail:* mxera@snut.edu.cn; minishiguang@126.com (L. Wang)

the electromagnetic parameters and spatial distribution of shielding materials, maintain high EMI SE while reducing surface reflection.[27] This offers a promising and effective solution to address the inherent trade-off between high EMI SE and low R in the field of EMI shielding.[28]

In the field of EMI shielding, the development of low-reflection EMI shielding materials faces dual challenges from both theoretical and engineering application perspectives. Theoretically, it is necessary to deeply explore the collaborative mechanism of dielectric loss and magnetic loss, and reveal the coupling laws between multi-scale electromagnetic parameters and interface polarization behavior. From the perspective of engineering application, it is essential to solve key issues such as lightweight structural design, wide frequency band, and large-scale production costs. Currently, it is crucial to develop EMI shielding materials with high EMI SE and low R. These materials address the precise electromagnetic protection needs of modern electronic devices and significantly promote advancements in the fields such as 5G communication, aerospace, and intelligent electronics.[29,30]

To address the existing research deficiencies and provide a comprehensive perspective, this review aims to systematically sort out and comment on the key progress and development trends in the field of low-reflection EMI shielding materials in recent years. Firstly, the shielding mechanism of low-reflection EMI shielding materials is briefly introduced. Subsequently, various advanced preparation techniques (such as freeze-drying, 3D printing, electroless plating, *etc*.) for achieving low-reflection characteristics are comprehensively summarized and compared, along with their advantages and disadvantages. Moreover, the key structural design strategies of low-reflection EMI shielding materials are emphasized and reviewed. Finally, the key scientific and technological problems of low-reflection EMI shielding materials are proposed, and the future development trends are discussed.

2. The low-reflection mechanism of EMI shielding

The shielding effect of materials is measured by SE, which refers to the attenuation of EMI energy within a certain frequency range. SE can be expressed as the logarithm of the ratio of incident power (P_i) to transmitted power (P_T), with the unit of dB.[31,32] In that case, SE can be expressed as follows:

$$SE(dB) = -\log\left(\frac{P_i}{P_T}\right) \quad (1)$$

The higher the SE, the stronger the ability of EMI materials to resist microwaves. According to Schelkunoff's theory, the total EMI shielding effectiveness (SE_T) can be represented as the sum of absorption loss (SE_A), reflection loss (SE_R), and multiple reflection loss (SE_M). The relationship can be described as follows:

$$SE_T = SE_R + SE_A + SE_M \quad (2)$$

When $SE_T > 15$ dB, SE_M can be disregarded. SE_R and SE_A can be further expressed as:

$$SE_R = 39.5 + 10log\frac{\sigma}{2\pi f\mu} \quad (3)$$

$$SE_A = 8.7d\sqrt{\pi f\mu\sigma} \quad (4)$$

In the formula, f represents the frequency of the EMWs (Hz); μ is the magnetic permeability of the material ($\mu = \mu_0\mu_r$, $\mu_0 = 4\pi\times10^{-7}$, μ_0 is the magnetic permeability of vacuum, μ_r is the relative magnetic permeability to vacuum ($H\cdot m^{-1}$); σ is the electrical conductivity of the material (S/m). It indicates that SE_R is affected by the ratio of σ/μ. Therefore, dielectric materials with extremely high σ and low μ usually exhibit high SE_R, and SE_A is a function of μ and σ, so both SE_R and SE_A increase with the increase of σ.

For low-reflection EMI shielding materials, R and absorption coefficient (A) can directly reflect the proportion of incident EMWs power that is reflected and absorbed. Therefore, by directly comparing the R and A of EMI shielding materials, it is easy to determine the dominant shielding mechanism: if R > A, it indicates that more incident EMWs are reflected and attenuated, with fewer EMWs enter the interior of the material, and thus less EMWs are absorbed and dissipated. That is to say, the shielding mechanism of this material is dominated by the reflection of EMWs. On the contrary, R < A implies that relatively fewer EMWs are reflected on the surface of the material, while more incident EMWs are absorbed and attenuated after enter the interior of the material, signifying that the shielding process of this material is mainly based on absorption.[33]

$$A = 1 - R - T \quad (5)$$

When transmission coefficient (T) is sufficiently small, the sum of A and R approaches 1, which indicates that directly comparing A or R with the critical value of 0.5 can also easily determine whether it is a low-reflection EMI shielding material. This judgment method is more applicable under the premise of $SE_T > 20$ dB ($T < 0.01$).

3. Preparation methods of EMI shielding composites with low reflection

The preparation method of low-reflection EMI shielding materials requires systematic design in combination with the EMI shielding mechanism. By precisely regulating the dielectric-magnetic performance parameters and structure of shielding materials, a balance between high EMI SE and low R can be effectively achieved. Currently, the main preparation methods include: Freeze-drying method, electroless plating method, vacuum-assisted filtration method, three-dimensional (3D) printing method, and electrospinning method. (Fig. 1)

3.1 Freeze-drying method

Freeze-drying is an advanced preparation method based on the principle of phase change.[34,35] The process involves freezing the water-containing material below the freezing point and then sublimating the ice under high vacuum conditions. The advantages lie in that the dried materials retain the original

chemical composition and microstructure, especially the 3D porous network structure resulting during the freezing process.[36,37] The freeze-drying method constructed a composite structure of "porous skeleton-conductive network-heterogeneous interface". On the one hand, the formed porous structure can significantly extend the propagation path of EMWs, enhance dielectric loss through multiple reflections and scattering, thereby improving EMI SE.[38-40] On the other hand, by inducing interface polarization loss, the dual goals of "low R-high EMI SE" are achieved.

Liu *et al*.[41] prepared (MXene@Ni/poly(p-phenylene-2,6-benzobisoxazole) nanofibers (PNF)-(MXene/PNF) aerogels through a layer-by-layer freeze-drying technique. When the mass ratio of MXene to Ni in MXene@Ni was 1:6 and the mass fraction of MXene in MXene/PNF was 80 wt%, the EMI SE of (MXene@Ni/PNF)-(MXene/PNF) aerogels achieved 71 dB with R as low as 0.10, realizing absorption-dominated shielding mechanism (Fig. 2(a-f)). Building upon the utilization of freeze-drying for aerogels but exploring a different post-treatment route, Zong *et al*.[42] fabricated MXene/cellulose nanofibers (CNF) aerogels by freeze-drying method, followed by high-temperature pyrolysis to produce TiC/C aerogels. Due to the porous structure and the abundant heterointerfaces between TiC and CNF, the TiC/C aerogels exhibited excellent EMI shielding performance. Specifically, when the mass fraction of MXene was 3 wt%, the EMI SE of TiC/C aerogels was up to 72.9 dB, and R was 0.24. Ma *et al*.[43] prepared porous 3D magnetic MXene/Fe_3O_4@acidified multi-walled carbon nanotubes (MFC) composite aerogels by directional freezing and freeze-drying. When the thickness was 2 mm, the EMI SE of MFC composite aerogels achieved 51.6 dB, and R was 0.31. Shifting the focus towards composite foams, Lei *et al*.[44] obtained silver fractal dendrites (AgFDs)/carbon nanotubes (CNT)/thermoplastic polyurethane (TPU) composite foams by layer-by-layer assembly combined with freeze-drying technology. When the thickness was 3.4 mm and the loadings of AgFDs was 0.103 vol%, the EMI SE of AgFDs/CNT/TPU composite foams was as high as 88.5 dB, while R was as low as 0.1. In our previous work,[45] $Ti_3C_2T_x$@CoNi/$Ti_3C_2T_x$/CNF composite foams (TCTCF) with asymmetric structure were prepared by layered freezing and freeze-drying technique. With a mass fraction of 50 wt% for $Ti_3C_2T_x$@CoNi, the EMI SE of TCTCF was up to 85 dB, and R was controlled between 0.22 and 0.47 (Fig. 2(g-o)).

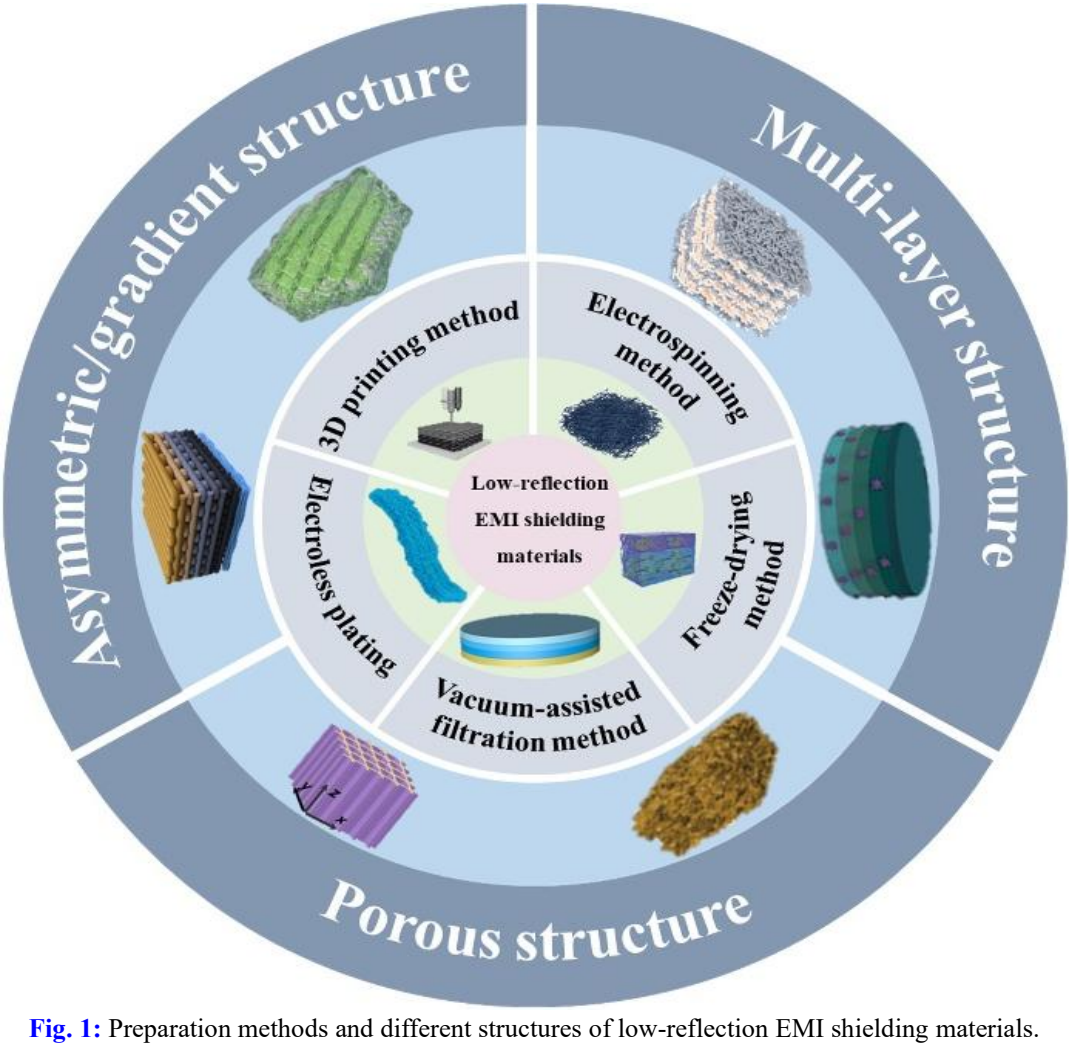

Fig. 1: Preparation methods and different structures of low-reflection EMI shielding materials.

.

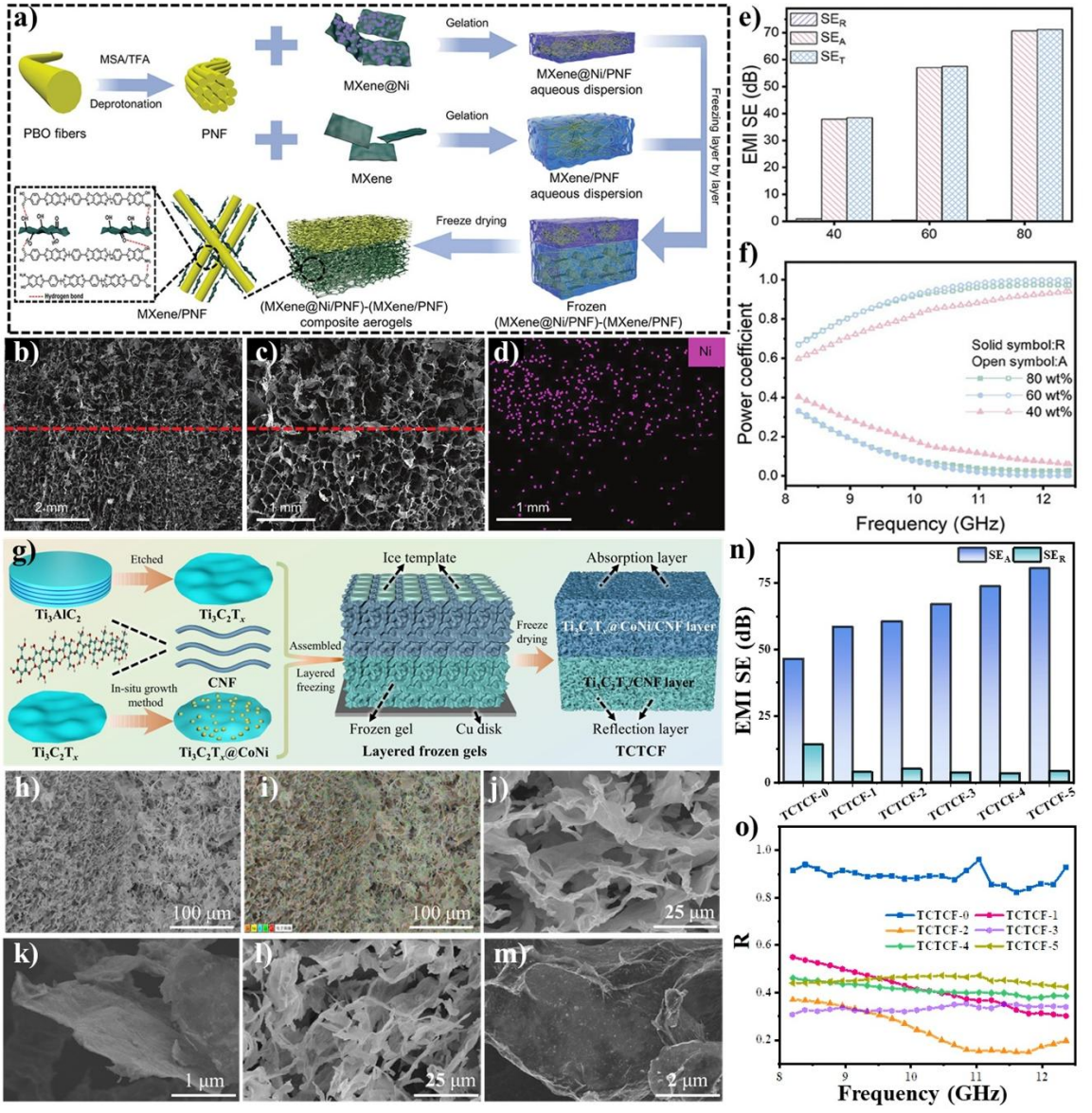

Fig. 2: a) Schematic illustration for preparation of (MXene@Ni/PNF)-(MXene/PNF) aerogels. b, c) SEM images of (MXene@Ni/PNF)-(MXene/PNF) aerogels and d) Ni element distribution, e) EMI SE, f) R and A of (MXene@Ni/PNF)-(MXene/PNF) aerogels. Reprinted with permission from Reference [41], Copyright 2024, Wiley-VCH. g) Schematic illustration of fabrication for TCTCF. h, i) SEM images of TCTCF, j, k) $Ti_3C_2T_x$/CNF layer and l, m) $Ti_3C_2T_x$@CoNi/CNF layers. n) EMI SE and o) R of TCTCF. Reprinted with permission from Reference [45], Copyright 2025, Elsevier.

3.2 Electroless plating method

Electroless plating refers to a coating method in which metal ions are reduced to metals by a reducing agent at room temperature without the application of an external current and deposited on the surface of the substrate. Compared with electroplating, electroless plating technology has the advantages of uniform coating, small pinholes, no need for direct current power supply equipment, and no restrictions on the material and shape of the substrate. By forming functional metal coatings (such as Ni, Cu, Ag) on the surface of non-conductive or weakly conductive substrates through electroless plating, the materials are endowed with excellent σ and magnetic permeability, thereby efficiently achieving reflection and absorption of EMWs.[46,47] Electroless plating, by preparing a highly conductive metal layer, works in concert with gradient conductive structures and porous electromagnetic loss layers to form a "low R-high EMI SE" shielding mechanism, thereby optimizing EMI shielding performance.

Tang *et al.*[48] prepared Fe_3O_4/Ag-loaded polyimide (PI) nonwoven fabrics (PFA)/pure Ag-coated PI nonwoven fabrics (PA) composites by in situ growth of Fe_3O_4 magnetic particles and electroless Ag plating process. When the Ag plating time for PFA and for PA were 1 h and 1.5 h, the EMI SE of PFA/PA composites reached 77 dB, and R was as low as 0.09 (Fig. 3(a-f)). Similarly, Zhao *et al.*[49] fabricated Fe_3O_4/Ag/PI (FAP) fabrics by in-situ growing Fe_3O_4/Ag nanoparticles on the PI surface and performing electroless Ag plating. Finally, the

FAP fabrics were assembled with Cu/Ni mesh (CN) to prepare FAP/CN fabrics. Notably, at a thickness of only 430 μm and a low density of 0.37 g/cm^3, the EMI SE of FAP/CN fabrics was up to 58 dB in the 24-40 GHz, and R was only 0.26. In a more complex process, Xu *et al.*[50] deposited nickel-plated aramid paper (NiP) through an electroless Ni plating process, and then fabricated Fe_3O_4/graphite particles (GP)/polydimethylsiloxane (PDMS) impregnated and polymerized polypyrrole (PPy) coated melamine foam layer (PGF-FL-NiP) composites. With a thickness of 2 mm, the EMI SE and R of PGF-FL-NiP composites were 62 dB and 0.23, respectively (Fig. 3(g-i)).

3.3 Vacuum-assisted filtration method

Vacuum-assisted filtration applies negative pressure on hydrophilic microporous filter membranes.[51,52] The process removes solvents from the mixed solution of conductive fillers and polymer matrices through a pressure difference. This process can precisely control the microstructure of EMI shielding materials with excellent interface interaction to achieve high performance.[53] The core of vacuum-assisted filtration technology lies in precisely constructing an electromagnetic gradient structure. Through layered design, impedance matching is optimized (to reduce reflection), and the "absorption-reflection-reabsorption" mechanism and interface polarization loss (to enhance absorption) are utilized. Ultimately, the shielding requirement of "dominant absorption" is met.

Guo *et al.*[54] fabricated $CoFe_2O_4$@MXene-silver nanowires (AgNWs)/CNF composite films via vacuum-assisted filtration technology. With a thickness of 0.1 mm, the EMI SE of $CoFe_2O_4$@MXene-AgNWs/CNF composite films was up to 84.3 dB, and R was 0.42 (Fig. 4 (a-g)). Similarly, Kim *et al.*[55] fabricated MXene/polyvinyl alcohol (PVA)/polyacrylic acid (PAA)-Hanji (MPP-H) textiles via vacuum-assisted filtration technology. When the MPP content was 2.77 mg cm^{-2}, the EMI SE of MPP-H textiles was 42 dB, and R was 0.45 (Fig. 4 (h-k)). In terms of structural design

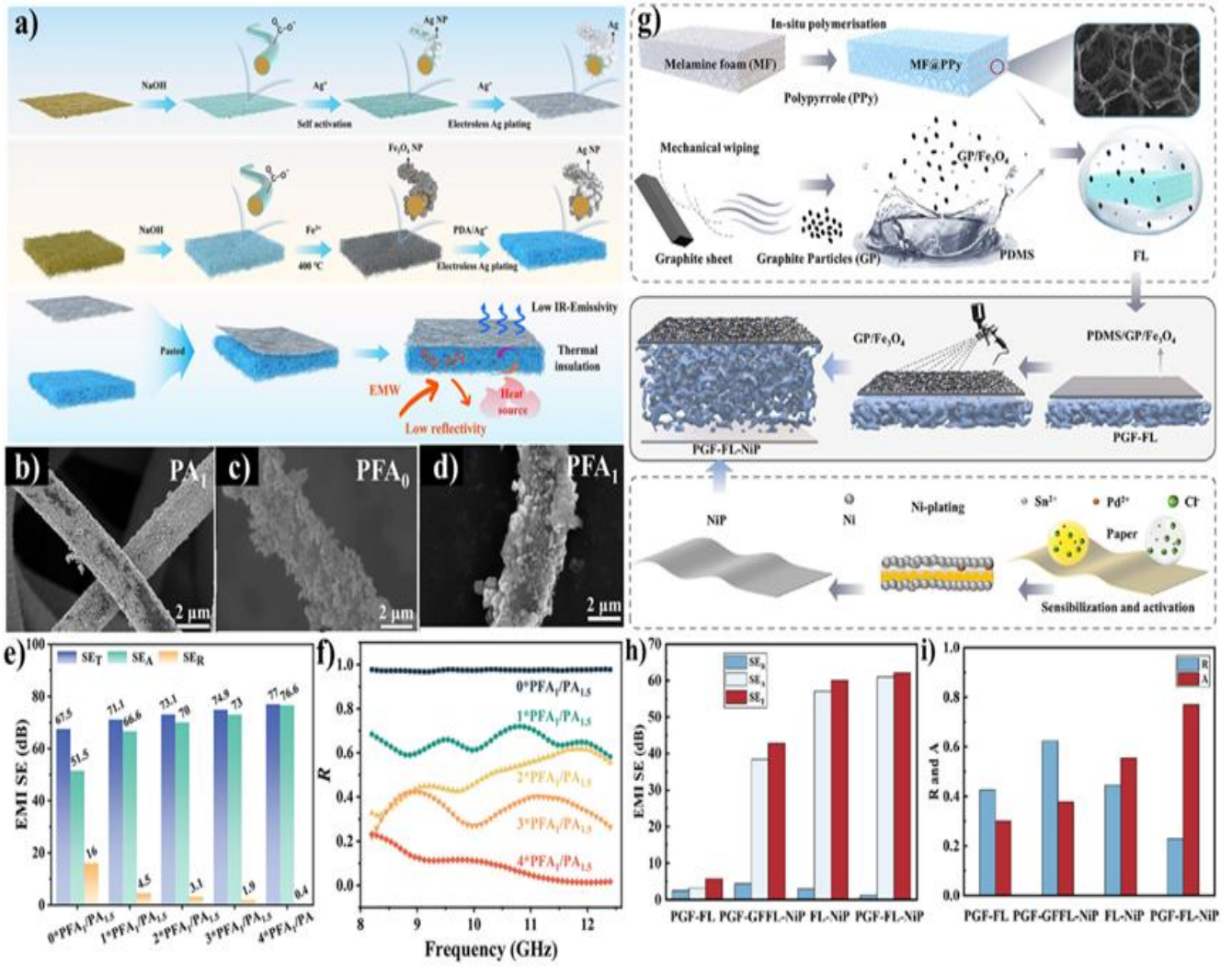

Fig. 3: a) Schematic illustration of preparation process of PFA/PA composites. SEM images of b) PA, c, d) PFA, e) EMI SE and f) R of PFA/PA composites. Reprinted with permission from Reference [48], Copyright 2024, Springer. g) Schematic diagram of the preparation process of PGF-FL-NiP composites. h) EMI SE, i) R and A of PGF-FL-NiP composites. Reprinted with permission from Reference [50], Copyright 2024, American Chemical Society.

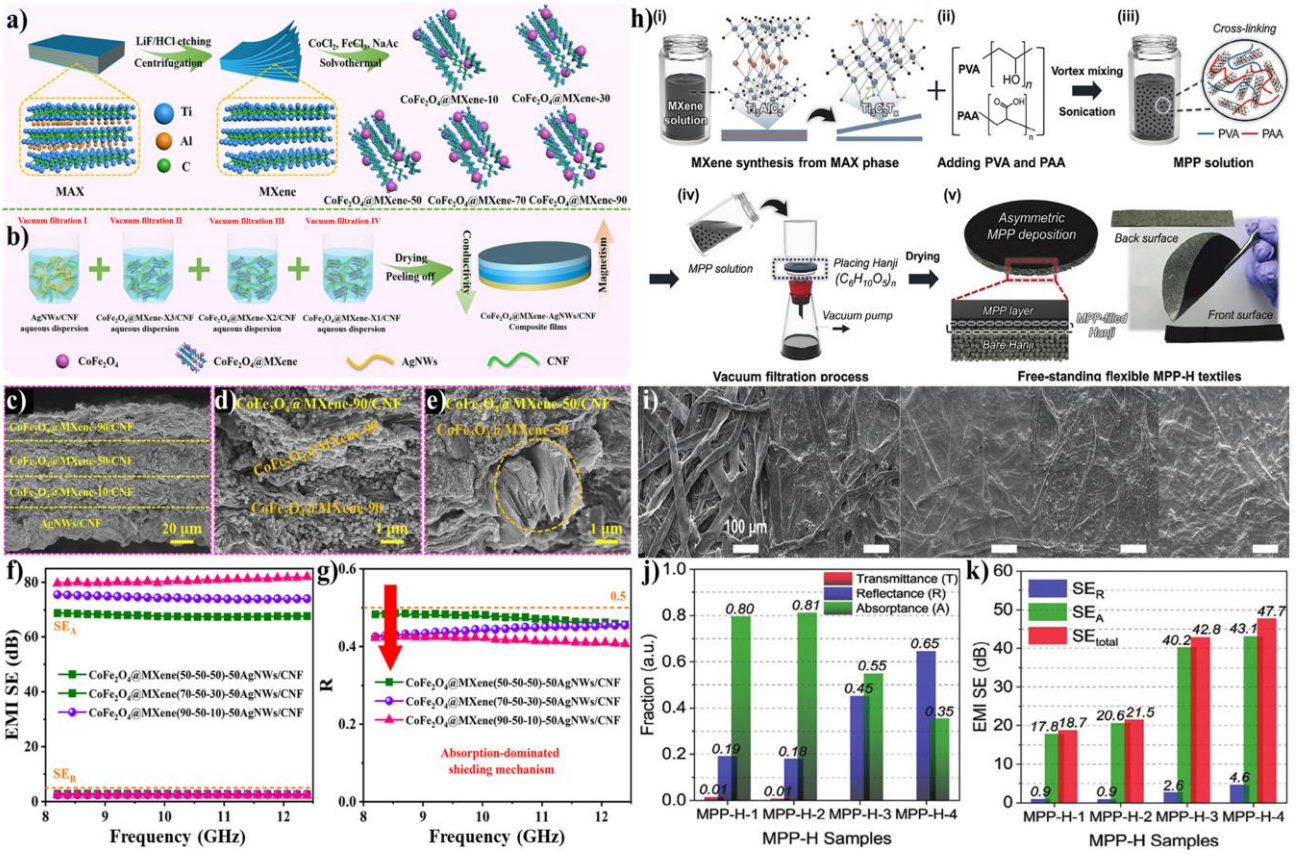

Fig. 4: a) Schematic illustration of fabrication process of $CoFe_2O_4$@MXene hybrids and b) $CoFe_2O_4$@MXene-AgNWs/CNF composite films. SEM images of c) $CoFe_2O_4$@MXene-AgNWs composite films d, e) $CoFe_2O_4$@MXene-CNF layer. f) EMI SE and g) R of $CoFe_2O_4$@MXene-AgNWs/CNF composite films. Reprinted with permission from Reference [54], Copyright 2023, Elsevier. h) Preparation of MPP-H textiles. i) SEM images, j) T, R, A and k) EMI SE of MPP-H textiles. Reprinted with permission from Reference [55], Copyright 2024, Wiley-VCH.

and performance optimization, Ma *et al*.[56] employed a layer-by-layer vacuum-assisted filtration to fabricate MXene/FeCo/CNF composite films with controllable magnetic-conductive dual-gradient structure. With a thickness of 340 μm, the EMI SE of MXene/FeCo/CNF composite films reached 58 dB, and R was 0.61. Furthermore, Li *et al*.[57] utilized vacuum-assisted filtration technology to prepare carbon fibers (CF)@NiCo/PI films. When the thickness was 1.08 mm, the EMI SE of CF@NiCo/PI films was as high as 87 dB, and R was as low as 0.13.

3.4 3D printing method

3D printing technology, based on digital models, can customize the shape of polymer materials according to a certain layer thickness and predetermined stacking trajectory.[58,59] With 3D printing technology, it is expected to prepare conductive composites with excellent performance and designable shapes, meeting the EMI shielding application requirements in different scenarios.[60-62] 3D printing achieves the "low reflection-multiple absorption and dissipation" mechanism of EMWs by precisely designing gradient structures, constructing hierarchical porous networks and regulating the synergistic effects of materials, providing a new approach for the preparation of absorption-dominated EMI shielding materials.

Xue *et al*.[63] utilized 3D printing technology to continuously print MXene/CNT/ PAA composite inks with different CNT contents, and then prepared gradient-conductive MXene/CNT/PI (GCMCP) composite aerogels through freeze-drying and thermal imidization treatment. With a thickness of 5 mm, the GCMCP aerogels demonstrated excellent EMI SE up to 68.2 dB and an ultra-low R of 0.23 (Fig. 5(a-f)). Besides, Hou *et al*.[64] obtained a polylactic acid (PLA)@MWCNT/PDMS@carbonyl iron powder (CIP) composites with a ring-shaped electromagnetic synergistic structure by 3D printing and solution casting techniques. When the thickness was 0.4 mm, the EMI SE of PLA@MWCNT/PDMS@CIP composites was 31 dB, and R was 0.3 (Fig. 5(g-j)). On the exploration path of structural innovation and performance improvement, Zhang *et al*.[65] fabricated lattice-filler dual-gradient Fe_3O_4/CNT/polyurethane (PU)@MXene (DGFCP@M) composite frames by 3D printing technology. The DGFCP@M composite frames displayed an outstanding EMI SE of 72 dB and R as low as 0.38.

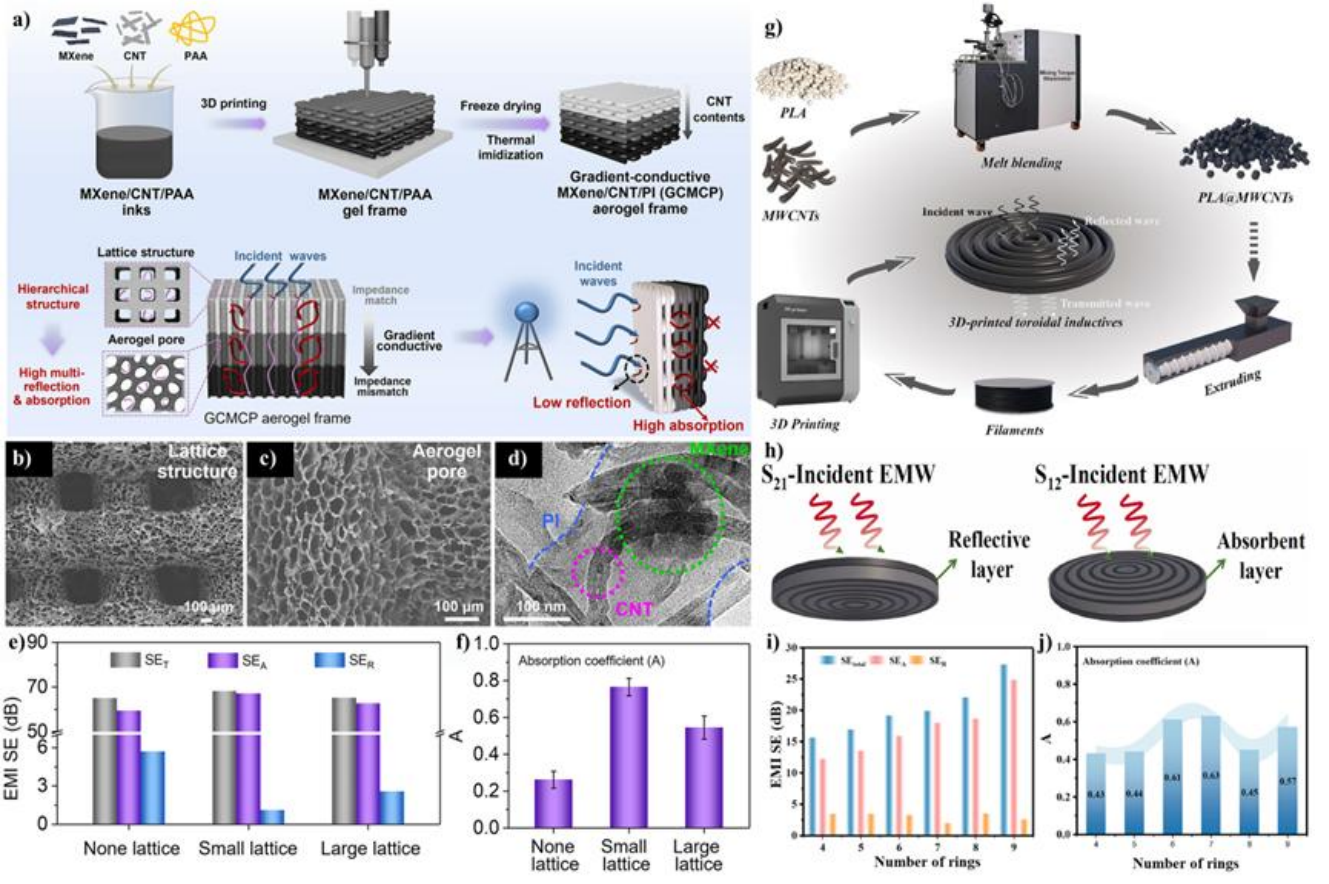

Fig. 5: a) Schematic illustration of fabrication process of the GCMCP aerogel frames. b, c) SEM images and d) TEM images of GCMCP aerogels. e) EMI SE and f) A of GCMCP aerogel frames with different lattice sizes. Reprinted with permission from Reference [63], Copyright 2023, Springer. g) Preparation of PLA@MWCNT filaments and the 3D-printed frameworks. h) Schematic diagram of incoming EMWs from different directions, i) EMI SE and j) A of PLA@MWCNT/PDMS@CIP composites. Reprinted with permission from Reference [64], Copyright 2024, Elsevier.

3.5 Electrospinning method

Electrospinning is a nanofiber preparation method based on the induction of an electric field. Its fundamental principle involves utilizing a high-voltage electrostatic field to induce charged jets from polymer solutions or melts, which subsequently solidify into fibers.[66-68] Nanofibers prepared by electrospinning have characteristics such as high aspect ratio, controllable porosity, and excellent mechanical properties. Electrospinning technology provides key support for EMI shielding materials to balance impedance matching and enhance EMWs absorption by constructing a multi-level structure of "continuous fiber network-porous morphology". Through the design of nanofiber structures and the combination of functional components, it has broken through the limitations of traditional EMI shielding materials, which are "thick, brittle, and narrow-band," and has shown significant value in the field of EMI shielding.[69,70]

Chen *et al*.[71] fabricated core-shell structured CP@PANI aerogels by freeze-drying and in situ growth of polyaniline (PANI) to coat carbon nanofibers (CNFs). When the thickness was 3 mm, the CP@PANI aerogels exhibited a remarkable EMI SE of 85.4 dB, corresponding to a low R of 0.43 (Fig. 6(a-d)). In contrast, focusing on stimuli-responsive materials, Tang *et al*.[72] used electrospinning technology with PAA as the precursor to in-situ introduce thermally expandable microspheres (EM), CNT and iron flakes (ZAF-5) into PI nonwoven fabrics (PMCZ). Finally, the PMCZ/liquid metal (LM) nonwoven fabrics were fabricated through chemical imidization, single-sided alkali treatment, and LM spraying process. Under a thermal stimulus of 170°C, the EMI SE of PMCZ/LM nonwoven fabrics was 57.5 dB, and R was 0.24. Meanwhile, utilizing waste materials, Gao *et al*.[73] prepared hydrolysate of waste leather scraps (HWLS)/polyacrylonitrile (PAN)/zeolitic imidazolate framework-67 (ZIF-67) nanofiber films through electrospinning technology. Finally, the Co@CNF@perfluorooctyltriethoxysilane (POTS) nanofiber films were successfully prepared by pre-oxidation, carbonization treatments and coating a POTS layer. With a thickness of 250 μm, the Co@CNF@POTS composite films exhibited an EMI SE of 49 dB and a low R of 0.43. Zhang *et al*.[74] prepared polydopamine (PDA)/silver nanoparticles (AgNPs)/MWCNT/Fe_3O_4 hybrid fillers (MFs) (TAMF) films via electrospinning technology. When the spray-coating times of PDMS/MFs was 3, the EMI SE of TAMF films was up to 85.4 dB, and R was 0.61 (Fig. 6(e-k)).

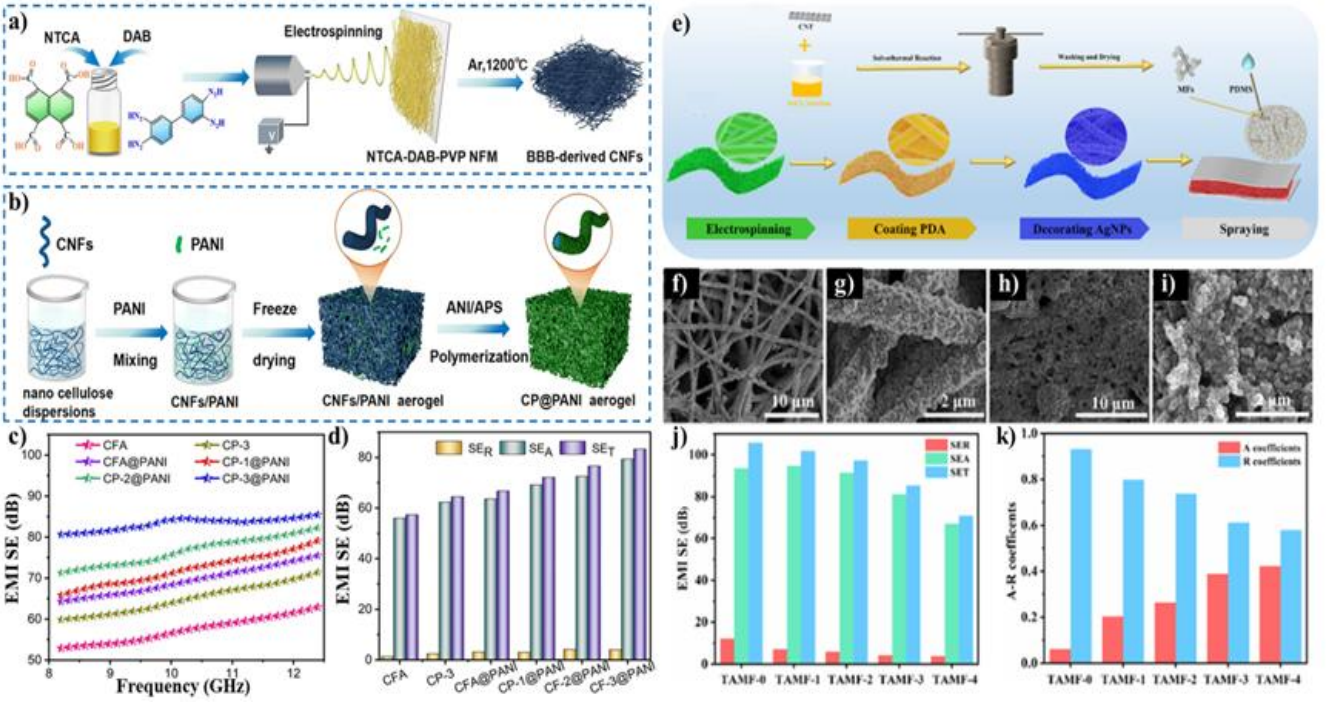

Fig. 6: a) Fabrication process of BBB nanofiber and b) CP@PANI aerogels, c) EMI SE and d) SE_R, SE_A, SE_T of CP@PANI aerogels. Reprinted with permission from Reference [71], Copyright 2025, Springer. e) Schematic diagram of the preparation process of TAMF films. f-i) SEM images of TAMF films. j) EMI SE, k) A and R of TAMF films. Reprinted with permission from Reference [74], Copyright 2022, ACS.

4. Structural design of low reflection EMI shielding materials

The key to the design of low-reflection EMI shielding materials lies in the coordinated optimization of structural regulation and loss mechanism, so as to achieve efficient EMWs absorption and impedance matching. Based on the microstructure, the structural design of low reflection EMI shielding materials can be classified into three ways: 1) porous structures; 2) multi-layer structures and 3) asymmetric/gradient structures.

4.1 Low reflection EMI shielding materials with porous structure

The porous structure design can effectively construct 3D conductive and magnetic flux pathways with low filler content.[75] Through the reasonable regulation of the conductive network and the porous structure, EMWs are reflected multiple times within shielding materials and transformed into heat energy for dissipation, thereby enhancing the absorption loss.[76, 77] At the same time, it effectively reduces surface reflection, thereby achieving absorption-dominated EMI shielding performance.[78-80]

Chu *et al.*[81] fabricated a honeycomb-structured porous Fe_3O_4@PPy/PI composite foams by using chemical foaming and in-situ vapor deposition of PPy technology. Due to the 3D porous structure of PI foams and the excellent σ of PPy films, with only 20 wt% Fe_3O_4@PPy, the EMI SE of Fe_3O_4@PPy/PI composite foams was 41.1 dB, and R was 0.62. In contrast, aiming for both higher EMI SE and lower R, Zhu *et al.*[82] fabricated Fe_3O_4@CNT/MXene/cross-linked aramid nanofiber (c-ANF)/PI (FMAP) aerogels with a 3D ordered hierarchical porous structure by using the unidirectional freezing strategy. With a mass fraction of 8 wt% for both Fe_3O_4@CNT and MXene, the FMAP aerogels achieved an excellent EMI SE of 67 dB and a low R of 0.14. Wang *et al.*[83] demonstrated an effective densification strategy to construct a compact porous structure of carbon black/graphene/Ni PI foams (CGNPF). With a thickness of 2 mm, the EMI SE of CGNPF was 44 dB, and R was as low as 0.29 (Fig. 7(a-g)). Building upon porous structure design but achieving significantly higher EMI SE across a broad frequency range, Mao *et al.*[84] adopted ice crystal dissolution/regeneration and atmospheric pressure drying strategy to prepare a cellulose-based composite aerogels (CNA) with discontinuous pores structures through layer-by-layer freeze casting. The CNA achieved an ultra-high EMI SE exceeding 90 dB and an ultra-low R of 0.2 across a wide band (1-18 GHz) (Fig. 7(h-l)). Wei *et al.*[85] constructed natural rubber (NR)/Fe_3O_4@CNT/expandable polymer microsphere (EPM) (NMCE) foam via latex mixing followed by template method. With a thickness of 2 mm, the NMCE foams achieved EMI SE of 30 dB and R of 0.28. Further exploring the versatility of freeze-drying for creating porous architectures, Ghosh *et al.*[86] prepared P-doped MXene/poly(3,4-ethylenedioxythiophene):poly(styrenesulfonate)(PEDOT:PSS) (MXP@PP) aerogels with a porous structure by freeze-drying process. With a mass fraction of MXP at 10 wt%, the EMI SE and R of MXP@PP aerogels were 40 dB and 0.4, respectively.

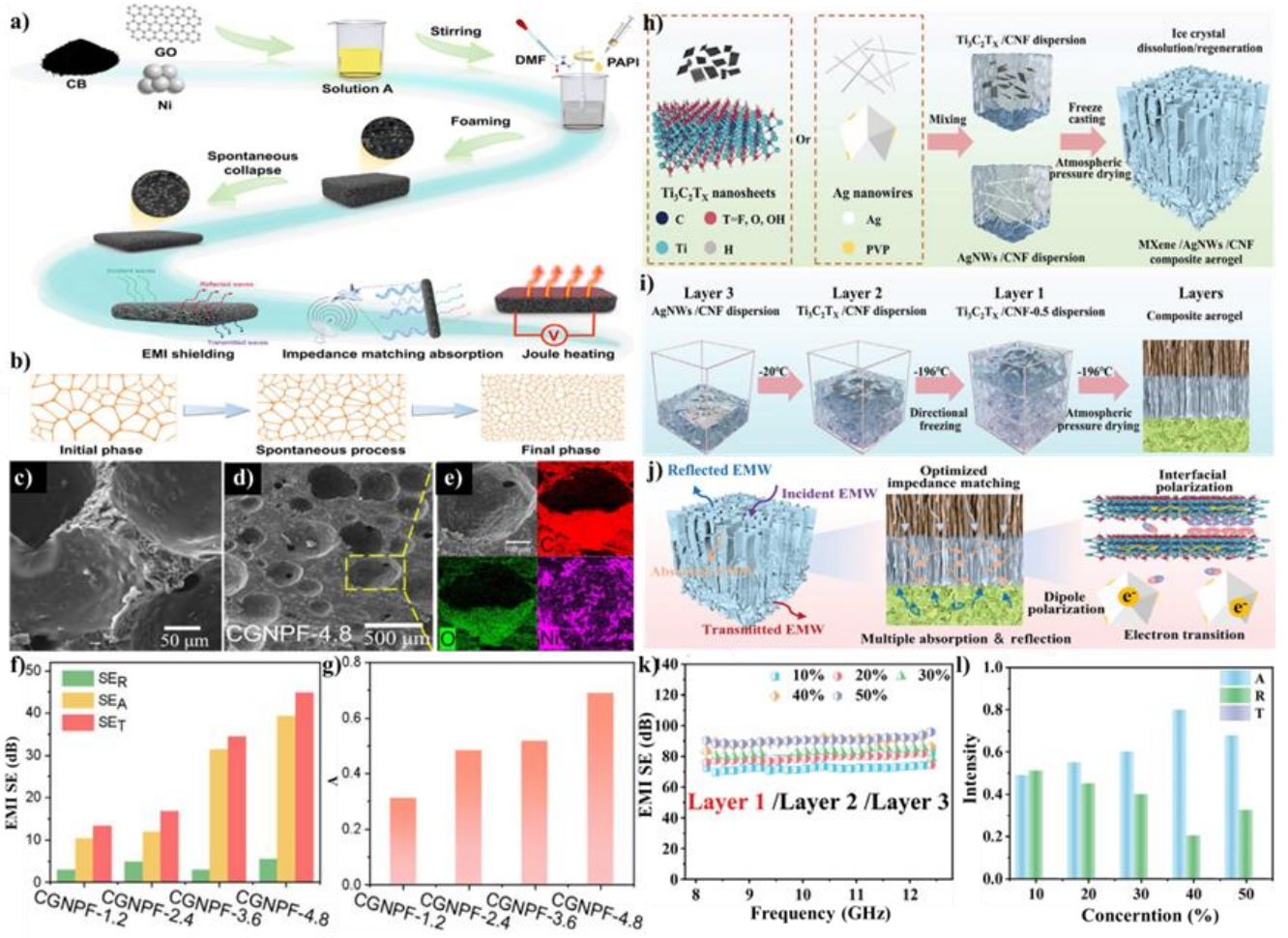

Fig. 7: a) Schematic diagram of preparation process of CGNPF and b) the cells of the "collapse densification" process. c, d) SEM images and e) C, O, Ni element distribution of CGNPF. f) EMI SE and g) A of CGNPF. Reprinted with permission from Reference [83], Copyright 2025, Elsevier. h) Preparation process illustrations and performance demonstration of the CNA. i) Ice crystal dissolution/regeneration strategy for the design of discontinuous pore gradients. j) The ultra-low reflection mechanism of CNA. k) EMI SE, l) A, R, and T of CNA. Reprinted with permission from Reference [84], Copyright 2025, Wiley-VCH.

The core advantage of the porous structure design lies in its excellent impedance matching and enhanced internal loss mechanism, while also offering benefits such as lightweight and potential breathability. However, its inherent limitation is weak mechanical strength. The current main challenges are focused on accurate and efficient theoretical modeling, optimization of wideband strong absorption, improvement of low-frequency performance, and cost control and large-scale production.

4.2 Low reflection EMI shielding materials with multi-layer structure

In the field of EMI shielding, multi-layer structure is an effective strategy to optimize EMI shielding performance.[87] Through reasonable design and integration of different functional layers, this multi-layer structure can not only achieve superior EMI SE, but also endow shielding materials with multifunctional properties such as thermal management, corrosion resistance, and stretchability, demonstrating broad application prospects.[88]

Chen *et al.*[89] fabricated reduced graphene oxide@fabric/graphene films (rGO@F/GF) by an evaporation-induced self-assembly strategy in combination with a centrifugal-assisted dip-coating method. At a thickness of less than 0.8 mm, the EMI SE of rGO@F/GF achieved 80 dB, and R was 0.172. In contrast, pursuing similar goals but through a divergent material system and approach, Mai *et al.*[90] prepared magnetic zeolitic imidazolate frameworks (ZIFs)-derived hollow CoNi carbon nanocage/MXene/nanocellulose bilayer (BZMN) aerogels by a two-step freezing method. When the mass fraction of MXene was 75 wt%, the EMI SE of BZMN aerogels was 35 dB, and R was 0.28 (Fig. 8(a-g)). Similarly exploring composite films but employing different techniques, Cheng *et al.*[91] fabricated sandwich-structured polyacrylate (PEA) composite films by spray coating and layer-by-layer casting (LBL-casting) techniques. With a mass fraction of 6 wt% for Fe_3O_4, the EMI SE of Fe_3O_4/MWCNT/Fe_3O_4 composite films reached 38.2 dB, and R was 0.44. Xu *et al.*[92] fabricated CF/graphene fibers (GF)/PDMS composite films with a double-layer

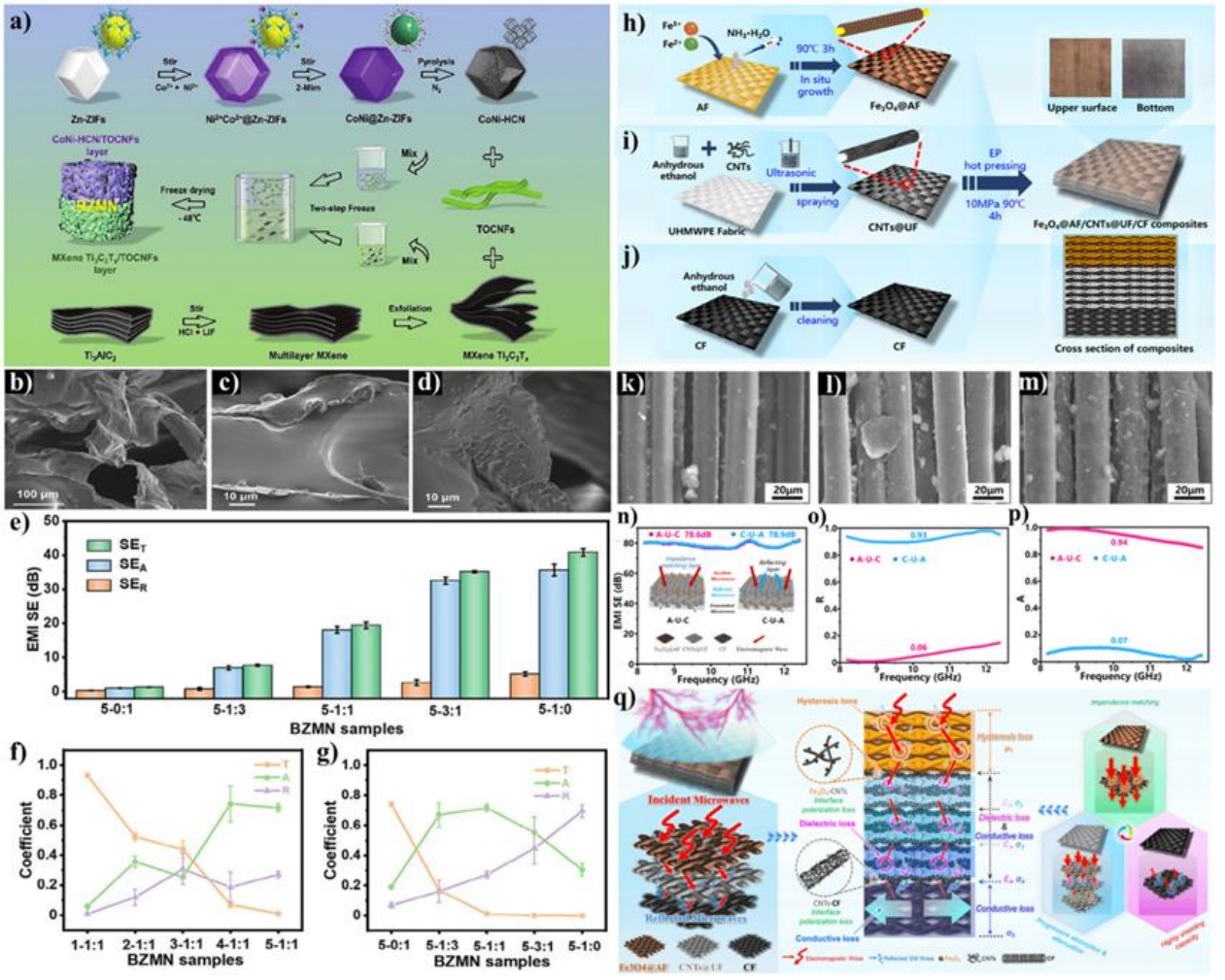

Fig. 8: a) Schematic diagrams of the preparation of BZMN aerogels. SEM images of the b) pore structure, c) lower layers, and d) upper layers of BZMN aerogels. e) EMI SE, f, g) T, A and R of BZMN aerogels. Reprinted with permission from Reference [90], Copyright 2024, Wiley-VCH. h) Fe_3O_4@AF fabrics prepared by in-situ growth method. i) CNT@UF fabrics prepared by spraying method. j) Treatment of woven CF. k-m) SEM images of the CNT@UF fabrics. n) EMI SE, o) R and p) A of the Fe_3O_4@AF/CNT@UF/CF composites. q) Schematic of the shielding mechanism for Fe_3O_4@AF/CNT@UF/CF composites. Reprinted with permission from Reference [93], Copyright 2023, Elsevier.

conductivenetwork structure by using solution casting techniques. When the mass fraction of CF and GF were 0.01 wt% and 1.00 wt%, the EMI SE of CF/GF/PDMS composite films reached 34 dB, and R was as low as 0.018. Shifting focus towards achieving exceptionally low reflection, Chang *et al*.[93] fabricated Fe_3O_4 decorated aramid fiber (AF)/CNT modified ultra-high molecular weight polyethylene (UHMWPE) fiber/CF (Fe_3O_4@AF/CNT@UF/CF)/epoxy composites by using a progressive conductive modular assembly strategy. When the number of layers of Fe_3O_4@AF, CNT@UF and CF fabrics were 4, 6 and 4 respectively. The EMI SE of Fe_3O_4@AF/CNT@UF/CF composites achieved 78.6 dB, and R was as low as 0.05 (Fig. 8(h-q)). Further advancing the design of high-performance and flexible EMI shielding textiles, Chen *et al*.[94] fabricated multifunctional flexible multilayered AgNPs/AgNWs/MXene/FeCo-C (AgDMC) textiles by using a noval multilayer self-assembly strategy. After being immersed in MXene and FeCo-C suspensions, the AgDMC textiles exhibited excellent EMI SE of 88 dB, with R as low as 0.168. This work provided a new strategy for low-reflection and absorption-dominant EMI shielding materials.

The multi-layer structure, with its advantages of wideband impedance matching, functional layer synergy, and low-frequency performance improvement, has demonstrated its value in flexible electronics, military stealth, and EMI shielding of precision equipment through the "surface impedance matching-internal strong attenuation" and "conductive-magnetic-conductive" layering design. However, it has limitations such as large thickness and weight, interface issues, and complex processes. Currently, it is necessary to overcome challenges such as ultra-thinness, material integration, and interface control, and promote its application in high-end electronics and national defense fields through material modification and intelligent design.

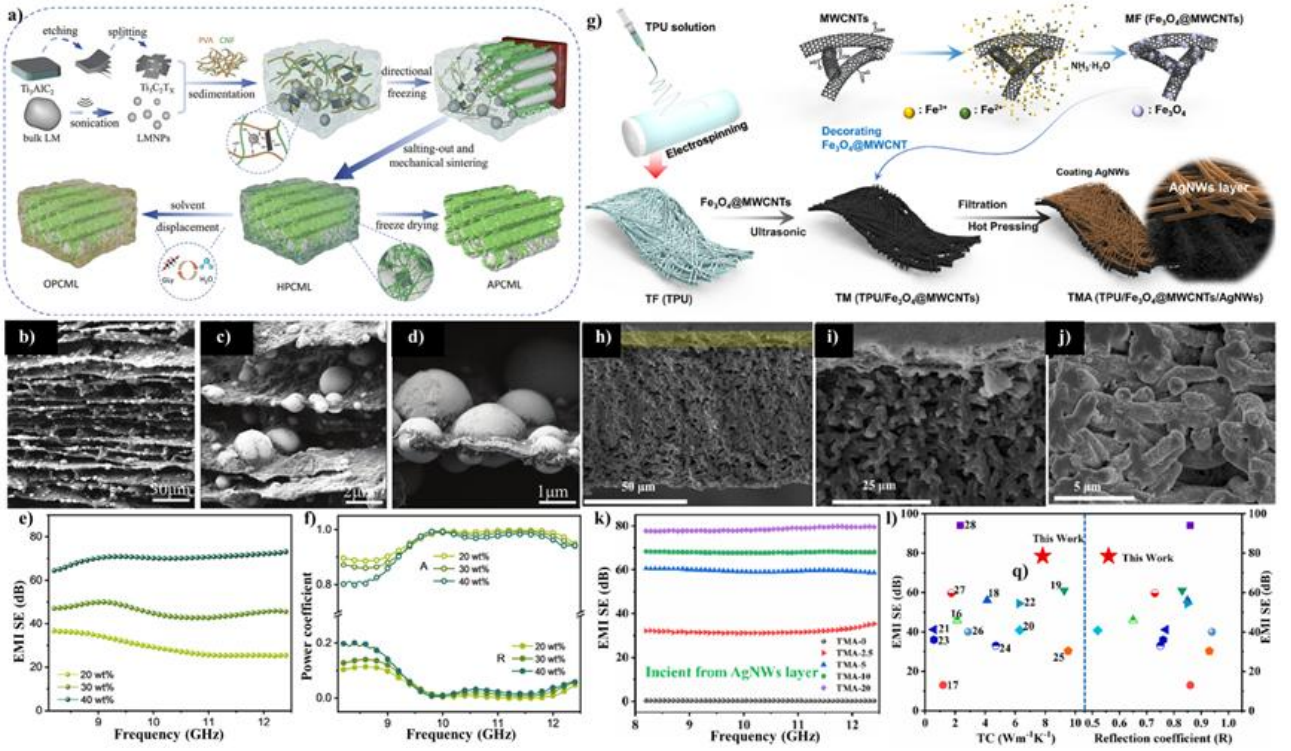

Fig. 9: a) Schematic illustration of preparation process of APCML. b-d) SEM images of APCML aerogels. e) EMI SE, and f) power coefficient of APCML aerogels. Reprinted with permission from Reference [101], Copyright 2024, Wiley-VCH. g) Schematic illustration for fabrication procedure of TMA composite films. h-j) SEM images of TMA composite films. k) EMI SE of TMA composite films. l) EMI SE vs R and EMI SE vs thermal conductivity (TC) comparisons of TMA composite films with different polymer composites reported in previous work. Reprinted with permission from Reference [102], Copyright 2023, Elsevier.

4.3 Low reflection EMI shielding materials with asymmetric/gradient structure

Asymmetric/gradient structure refers to the structure in which the conductivity of each layer varies irregularly or increases gradually along the direction of EMWs incidence. The main factors affecting the EMI SE of asymmetric/gradient structure are the σ of the conductive layer, absorbing layers and the direction of EMWs incidence.[95-97] The asymmetric/gradient conductive structure forms an absorption-reflection-reabsorption interface for EMWs, endowing the material with excellent EMI shielding performance dominated by absorption.[98,99]

Qian *et al.*[100] fabricated TPU/CNT/Fe_3O_4-decorated rGO/Ag composite foams (TCFAs) with an asymmetric structure by a supercritical CO_2 foaming process and thermal stretching. With a filler content as low as 1.784 vol%, the EMI SE of TCFAs was up to 89.5 dB, and R as low as 0.253. Similarly focused on achieving high EMI SE with low R through structural design, He *et al.*[101] integrated MXene and liquid metal nanoparticles (LMNPs) into a dual-network structure composed of PVA and CNF. By taking advantage of gravity-induced natural sedimentation of LMNPs. Finally, the asymmetric gradient-structured PVA/CNF/MXene/LM (APCML) aerogels were prepared. When the thickness was 3 mm, the EMI SE of APCML aerogels achieved 71 dB with R only 0.064, demonstrating a compatible balance between shielding and microwave absorption performance (Fig. 9(a-f)). In a different approach utilizing hybrid fillers and surface modification, Zhang *et al.*[102] ultrasonically adsorbed the hybrid filler of MWCNT and Fe_3O_4 (MFs) onto the surface of TPU fibers and then attached a layer of AgNWs to the TPU/Fe_3O_4@MWCNT fiber films using vacuum-assisted filtration technology. Finally, the TPU/MFs/AgNWs (TMA) composite films were prepared. When the amount of AgNWs was 2.7 wt% and the thickness was 78 μm, the EMI SE of TMA composite films reached as high as 78.48 dB, and R was 0.56. (Figs. 9(g-l)). Further exploring asymmetric structures but employing directional freezing, Yao *et al.*[103] obtained MXene/ANF/PI (AMAP) aerogels with an asymmetric structure through vacuum-assisted filtration technology and directional freezing casting process. Under the interaction of the layered MXene/ANF and porous AMAP structures, when the thickness was 15 mm, the EMI SE of AMAP aerogels was 47 dB, corresponding to a low R of 0.0138.

Gradient structures can achieve efficient broadband EMWs absorption at relatively thin thicknesses, but they still face challenges such as difficult interface bonding and theoretical model construction. Asymmetric structures can realize low reflection characteristics on one side of the material and integrate other functions (such as thermal conduction, magnetism, *etc.*) on the other side, making them suitable for directional electromagnetic control or thermal management

Table 1: Comparison for EMI shielding performance and R of low-reflection EMI shielding materials.

Samples	Thickness (mm)	EMI SE (dB)	R	Reference
MXene/Fe_3O_4@aMWCNT	2	51.6	0.31	[44]
PI/Fe_3O_4/Ag/Cu/Ni	0.43	58	0.26	[49]
$CoFe_2O_4$@MXene-AgNWs/CNF	0.1	84.3	0.42	[54]
MXene/FeCo/CNF	0.34	58	0.61	[56]
CF@NiCo/PI	1.08	87	0.13	[57]
MXene/CNT/PI	5	68.2	0.23	[63]
PLA@MWCNT/PDMS@CIP	0.4	31	0.3	[64]
Co@CNF@POTS	0.25	49	0.43	[73]
Fe_3O_4@PPy/PI	8	41.1	0.8	[81]
Carbon/graphene/Ni PI	2	44	0.29	[83]
PVA/CNF/MXene/LM	3	71	0.064	[101]
TPU/MFs/AgNWs	0.078	78.4	0.56	[102]
MXene/ANF/PI	15	47	0.013	[103]
PVDF/SiCNW@MXene/PVDF/CNT	3.8	45	0.03	[104]
LM-coated textile	1	49	0.4	[105]
LM/elastomeric polymer	2	66	0.5	[106]
Waterborne polyurethane foam	4	84	0.08	[107]
Ni/MXene/melamine foam	2	34.6	0.16	[108]

scenarios. However, when designing, the mutual influence of the performance on both sides needs to be taken into account, and higher requirements are placed on the interface bonding strength and material compatibility. These two structures still face challenges in terms of preparation processes, performance stability, *etc*., and their commercialization needs to be promoted through material innovation, process optimization and theoretical improvement.

Table 1 presents a comparative analysis of the EMI SE and R of different types of low-reflection EMI shielding materials. The table selects representative conductive polymer-based composites, metal-based composites, carbon-based composites, and novel nano-composite shielding materials from current research as the research objects.

5. Summary and perspective

This review summarizes the shielding mechanisms and preparation methods of low-reflection EMI shielding materials, and the latest research progress in low-reflection EMI shielding materials with different structures is reviewed. Although researchers have made great progress in the preparation of low-reflection EMI shielding materials, most of these materials are not suitable for large-scale production due to harsh preparation conditions (complex processes, high costs, and long time consumption). The primary advantage of the freeze-drying method is the preservation of the original chemical composition and micro-porous structure. However, the drying process takes a long time and the material size is limited. The electroless plating method is simple and environmentally friendly, but it is difficult to control the uniformity of coating thickness. The vacuum-assisted filtration method can form a dense structure to achieve superior EMI SE with a low thickness; however, it is usually suitable for small samples, and uniform film formation over a large area requires process optimization. 3D printing technology can prepare EMI shielding materials with complex 3D structures, achieving synergistic regulation of impedance matching and multiple scattering. However, the equipment

cost of this technology is relatively high, and the available printing material systems are rather limited. Electrospinning can prepare nanofiber with high specific surface area and interface polarization that enhance EMWs loss. However, it has strict requirements for environmental temperature, humidity, cleanliness as well as fiber morphology being easily affected by fluctuations in process parameters.

Therefore, exploring and developing new preparation and processing methods, simplifying the process, adjusting the product size, and reducing production costs are crucial for the development of low-reflection EMI shielding materials. To achieve EMI shielding materials with both high EMI SE and low R, the materials need to optimize the multiple loss paths of EMWs through structural design while reducing surface reflection. The design of porous structures can increase the scattering and interface polarization losses of EMWs, while reducing direct surface reflection. Although the introduction of porous structures can improve impedance matching (reduce surface reflection), excessive pursuit of low reflection may sacrifice overall EMI SE. Multilayer structures reduce the reflection of incident waves by alternately stacking functional layers with different electromagnetic properties and utilizing the impedance gradient matching between layers, while promoting multiple scattering and absorption of EMWs. However, the polymer matrix is separated by selectively distributed conductive fillers, which can lead to a decrease in the mechanical properties. Gradient/asymmetric structures achieve gradual impedance matching through continuous gradient changes in composition or porosity (such as increasing the concentration of conductive fillers along the thickness direction), allowing EMWs to gradually enter the shielding material and be absorbed rather than directly reflected. In the design of gradient/asymmetric structures, the thickness, component ratio, and porosity of the gradient layers need to be precisely matched. Otherwise, impedance matching may fail. Therefore, for the preparation of EMI shielding materials with both high EMI SE and low R, reasonable and efficient structural design is of vital importance.

Based on this, advanced preparation and processing methods (such as chemical vapor deposition (CVD) and microfluidic technology) should be developed, along with precise design for microstructure optimization based on low-reflection EMI shielding materials to achieve the collaborative optimization of various physicochemical properties of EMI shielding materials. At the same time, multiple preparation methods should be combined, such as 3D printing in conjunction with ice templating to prepare gradient porous-dense materials, further improving EMI SE. In addition, the relationship between shielding materials and EMWs should be explored to enhance understanding of the intrinsic EMI shielding mechanisms, which will greatly promote the development of the next generation of low-reflection EMI shielding materials.

In conclusion, the key to the development of low-reflection EMI shielding materials lies in innovative breakthroughs in preparation methods and precise control of microstructure, which is essential for driving them from laboratory research to industrial application. It is believed that low-reflection EMI shielding materials will evolve towards intelligence, sustainability, and multifunctionality. This new type of materials will play a crucial role in fields such as electronic communication, flexible wearable devices, and aerospace in the future.

Acknowledgments

This work was supported by the National Natural Science Foundation of China (52303090); The Innovation Capability Support Plan of Shaanxi Province (2024ZC-KJXX-022); The Youth Talent Promotion Project of Shaanxi Science and Technology Association (20240426); The Youth Innovative Team of Shaanxi Universities (No.2022.94).

Conflict of Interest

There is no conflict of interest.

Reference

[1] A. A. Isari, A. Ghaffarkhah, S. A. Hashemi, S. Wuttke, M. Arjmand, Structural design for EMI shielding: from underlying mechanisms to common pitfalls, *Advanced Materials*, 2024, **36**, 2310683, doi: 10.1002/adma.202310683.

[2] J. Wang, X. Wu, Y. Wang, W. Zhao, Y. Zhao, M. Zhou, Y. Wu, G. Ji, Green, sustainable architectural bamboo with high light transmission and excellent electromagnetic shielding as a candidate for energy-saving buildings, *Nano-Micro Letters*, 2022, **15**, 11, doi: 10.1007/s40820-022-00982-7.

[3] B. Park, S. Hwang, H. Lee, Y. Jung, T. Kim, S. J. Kwon, D. Jung, S.-B. Lee, Absorption-dominant electromagnetic interference (EMI) shielding across multiple mmWave bands using conductive patterned magnetic composite and double-walled carbon nanotube film, *Advanced Functional Materials*, 2024, **34**, 2406197, doi: 10.1002/adfm.202406197.

[4] S. Zhang, S. Zhang, P. Zhu, J. Li, Y. Li, C. Zhou, Q. Qiu, X. Jing, K.-W. Paik, P. He, Recent achievements and performance of nanomaterials in microwave absorption and electromagnetic shielding, *Advances in Colloid and Interface Science*, 2025, **335**, 103336, doi: 10.1016/j.cis.2024.103336.

[5] Y. Shi, S. Liao, Q. Wang, X. Xu, X. Wang, X.. Gu, Y. Hu, P. Zhu, R. Sun, Y. Wan, Enhancing the interaction of carbon nanotubes by metal–organic decomposition with improved mechanical strength and ultra-broadband EMI shielding performance, *Nano-Micro Letters*, 2024, **16**, 134, doi: 10.1007/s40820-024-01344-1.

[6] L. Wang, J. Cheng, Y. Zou, W. Zheng, Y. Wang, Y. Liu, H. Zhang, D. Zhang, X. Ji, Current advances and future perspectives of MXene-based electromagnetic interference shielding materials, *Advanced Composites and Hybrid Materials*, 2023, **6**, 172, doi: 10.1007/s42114-023-00752-y.

[7] L. Wang, Z. Yang, L. Lang, J. Men, T. Gao, Q. Wang, J. Cheng, Y. Liu, N. Zheng, J. Liu, X. Ji, Flexible multifunctional MXene/polyimide films with Janus structure for superior

electromagnetic interference shielding, *Advanced Composites and Hybrid Materials*, 2024, **8**, 26, doi: 10.1007/s42114-024-01100-4.
[8] J. Chen, Y. Zhang, H. Li, W. Feng, X. Gao, D. Yao, H. Wu, H. Wang, T. You, C. Lu, X. Pang, Recyclable polymer composites with a wrinkled core-shell structure for highly efficient EMI shielding and low reflection, *ACS Applied Materials & Interfaces*, 2024, **16**, 25148-25159, doi: 10.1021/acsami.4c04426.
[9] L. Wang, L. Chen, P. Song, C. Liang, Y. Lu, H. Qiu, Y. Zhang, J. Kong, J. Gu, Fabrication on the annealed $Ti_3C_2T_x$ MXene/Epoxy nanocomposites for electromagnetic interference shielding application, *Composites Part B: Engineering*, 2019, **171**, 111-118, doi: 10.1016/j.compositesb.2019.04.050.
[10] H. Lee, S. H. Ryu, S. J. Kwon, J. R. Choi, S.-B. Lee, B. Park, Absorption-dominant mmWave EMI shielding films with ultralow reflection using ferromagnetic resonance frequency tunable M-type ferrites, *Nano-Micro Letters*, 2023, **15**, 76, doi: 10.1007/s40820-023-01058-w.
[11] Z. Ma, J. He, S. Liu, W. Zhang, M. Gan, Q. Wu, M. Xing, Adjustable humidity response: ultrahigh green EMI shielding gel with double-side constant temperature capability, *Advanced Functional Materials*, 2025, **35**, 2414942, doi: 10.1002/adfm.202414942.
[12] C. Xiong, Q. Xiong, M. Zhao, B. Wang, L. Dai, Y. Ni, Recent advances in non-biomass and biomass-based electromagnetic shielding materials, *Advanced Composites and Hybrid Materials*, 2023, **6**, 205, doi: 10.1007/s42114-023-00774-6.
[13] L. Wang, L. Lang, X. Hu, T. Gao, M. He, H. Qiu, X. Ji, H. Guo, Y. Zhang, S. Huang, Multifunctional ionic bonding-strengthened ($Ti_3C_2T_x$ MXene/CNF)-(BNNS/CNF) composite films with Janus structure for outstanding electromagnetic interference shielding and thermal management, *Journal of Materials Science & Technology*, 2025, **224**, 46-55, doi: 10.1016/j.jmst.2024.11.010.
[14] C. Xiong, C. Zheng, Z. Zhang, Q. Xiong, Q. Zhou, D. Li, M. Shen, Y. Ni, Polyaniline@cellulose nanofibers multifunctional composite material for supercapacitors, electromagnetic interference shielding and sensing, *Journal of Materiomics*, 2025, **11**, 100841, doi: 10.1016/j.jmat.2024.01.015.
[15] L. Wang, Z. Yang, X. Hu, H. Qiu, B. Xiang, H. Guo, Y. Zhang, X. Ji, Multifunctional polyethylene terephthalate fabrics with multilevel conductive networks for electromagnetic interference shielding and photothermal conversion, *Nano Research*, 2025, **18**, 94907500, doi: 10.26599/nr.2025.94907500.
[16] G. Liu, J. Li, D. Yin, H. Xiu, S. Wang, X. Jiang, Y. Qin, F. Hua, Y. Jia, M. Shen, Electromagnetic bilayer composite film: Cocoa-tree-like FL and spiky-ball-like CN structures for superior electromagnetic shielding, thermal management, and strain sensing performance, *Chemical Engineering Journal*, 2025, **512**, 162638, doi: 10.1016/j.cej.2025.162638.
[17] L. Wang, Z. Ma, Y. Zhang, H. Qiu, K. Ruan, J. Gu, Mechanically strong and folding-endurance $Ti_3C_2T_x$ MXene/PBO nanofiber films for efficient electromagnetic interference shielding and thermal management, *Carbon Energy*, 2022, **4**, 200-210, doi: 10.1002/cey2.174.
[18] J. Zhou, Y. Zhu, K. Qian, M. Miao, X. Feng, Poly(3, 4-ethylenedioxythiophene): sulfamic acid modified aramid nanofibers: an innovative conductive polymer with enhanced electromagnetic interference shielding and thermoelectric performance, *Small*, 2024, **20**, 2405400, doi: 10.1002/smll.202405400.
[19] L. Wang, L. Lang, W. Ren, Z. Yang, T. Gao, Z. Zhao, M. Kallel, Y. Liu, Electrically insulating composite films with excellent electromagnetic interference shielding performance enabled by multilayer structure, *Engineered Science*, 2025, **34**, 1477, doi: 10.30919/es1477.
[20] Z. Ma, R. Jiang, J. Jing, S. Kang, L. Ma, K. Zhang, J. Li, Y. Zhang, J. Qin, S. Yun, G. Zhang, Lightweight dual-functional segregated nanocomposite foams for integrated infrared stealth and absorption-dominant electromagnetic interference shielding, *Nano-Micro Letters*, 2024, **16**, 223, doi: 10.1007/s40820-024-01450-0.
[21] J. Feng, Y. Bai, P. Wang, X. Chen, S. Han, H. Liu, X. Luo, P. Zhang, X. Wang, J. Liu, Zr^{4+} and Al^{3+} coordinated cross-linked conductive collagen fibers/solvent-free polyurethane foam with ultra-low reflective electromagnetic shielding properties, *Chemical Engineering Journal*, 2024, **499**, 156695, doi: 10.1016/j.cej.2024.156695.
[22] X. Jia, Y. Li, B. Shen, W. Zheng, Evaluation, fabrication and dynamic performance regulation of green EMI-shielding materials with low reflectivity: a review, *Composites Part B: Engineering*, 2022, **233**, 109652, doi: 10.1016/j.compositesb.2022.109652.
[23] L. Wang, H. Qiu, C. Liang, P. Song, Y. Han, Y. Han, J. Gu, J. Kong, D. Pan, Z. Guo, Electromagnetic interference shielding MWCNT-Fe_3O_4@Ag/epoxy nanocomposites with satisfactory thermal conductivity and high thermal stability, *Carbon*, 2019, **141**, 506-514, doi: 10.1016/j.carbon.2018.10.003.
[24] L. Xiang, D. Pan, J. Lei, N. AlMasoud, T. S. Alomar, I. G. Issaulu, Y. Wang, Z. M. El-Bahy, C. Liu, Z. Guo, S. Ainur, Z. Toktarbay, Sodium alginate aerogel derived SiC@Co-C 3D network enhances electromagnetic wave absorption and thermal conductivity of PDMS based composite, *International Journal of Biological Macromolecules*, 2025, **306**, 141539, doi: 10.1016/j.ijbiomac.2025.141539.
[25] Y. Zhao, N. Ahmad, Y. Yang, W. Zhai, Mechanical-dielectric optimized graphene aerogels with strain-tunable microwave attenuation and shielding functions, *Journal of Materials Chemistry A*, 2025, **13**, 325-339, doi: 10.1039/D4TA06820C.
[26] Z. Du, C. Zhou, H. Mi, H. Li, Z. Qin, R. Xu, Y. Wang, C. Liu, C. Shen, Recorded low-reflection in gradient MXene-decorated melamine microwave shielding foam integrated with piezoresistive sensing and energy absorption properties, *Composites Part A: Applied Science and Manufacturing*, 2023, **173**, 107694, doi: 10.1016/j.compositesa.2023.107694.
[27] L. Kong, S. Zhang, Y. Liu, H. Wu, X. Fan, Y. Cao, J. Huang, Hierarchical architecture bioinspired CNTs/CNF electromagnetic wave absorbing materials, *Carbon*, 2023, **207**, 198-206, doi: 10.1016/j.carbon.2023.03.024.
[28] Y. Xu, X. Zhang, G. Wang, X. Zhang, J. Luo, J. Li, S. Q. Shi,

J. Li, Q. Gao, Preparation of a strong soy protein adhesive with mildew proof, flame-retardant, and electromagnetic shielding properties *via* constructing nanophase-reinforced organic–inorganic hybrid structure, *Chemical Engineering Journal*, 2022, **447**, 137536, doi: 10.1016/j.cej.2022.137536.
[29] W. Zou, X. Zheng, J. Huang, G. Wang, Z. Guo, Recent advances in injection molding of carbon fiber reinforced thermoplastic polymer composites: a review, *ES General*, 2023, **1**, 938, doi: 10.30919/esg938.
[30] J. Men, B. Xiang, X. Mao, W. Ren, Z. Yang, S. Zhang, L. Wang, Ultra-flexible and mechanically strong silver nanowires/PBO nanofibers composite films for thermal management and photothermal conversion, *Journal of Colloid and Interface Science*, 2025, **700**, 138352, doi: 10.1016/j.jcis.2025.138352.
[31] H. Liu, Y. Yang, N. Tian, C. You, Y. Yang, Foam-structured carbon materials and composites for electromagnetic interference shielding: Design principles and structural evolution, *Carbon*, 2024, **217**, 118608, doi: 10.1016/j.carbon.2023.118608.
[32] D. Li, C. Dong, A. P. Zhang, H. L. Lin, B. Y. Peng, K. Y. Ni, K. C. Yang, J. Bian, D. Q. Chen, Polymer-based composites for electromagnetic interference shielding: principles, fabrication, and applications, *Composites Part A: Applied Science and Manufacturing*, 2025, **194**, 108927, doi: 10.1016/j.compositesa.2025.108927.
[33] K. Qian, J. Zhou, M. Miao, S. Thaiboonrod, J. Fang, X. Feng, Stretchable supramolecular hydrogel with instantaneous self-healing for electromagnetic interference shielding control and sensing, *Composites Part B: Engineering*, 2024, **287**, 111826, doi: 10.1016/j.compositesb.2024.111826.
[34] J. Jiang, P. Zhou, Y. Yi, D. Chen, G. Hu, X. Liu, L. Tang, Dual-crosslinked network structured polybenzoxazine/PBO nanofiber aerogel with thermal insulation, flame retardancy, and super-hydrophobicity, *Polymer Degradation and Stability*, 2025, **234**, 111216, doi: 10.1016/j.polymdegradstab.2025.111216.
[35] H. Xiao, M. Yang, J. Lv, X. He, M. Chen, W. Tan, W. Yang, K. Zeng, J. Hu, G. Yang, Biomineralization-inspired confined-space fabrication of polyimide aerogels, *ACS Applied Materials & Interfaces*, 2024, **16**, 2763-2773, doi: 10.1021/acsami.3c15696.
[36] S. Li, J. Wang, Z. Zhu, D. Liu, W. Li, G. Sui, C. B. Park, CVD carbon-coated carbonized loofah sponge loaded with a directionally arrayed MXene aerogel for electromagnetic interference shielding, *Journal of Materials Chemistry A*, 2021, **9**, 358-370, doi: 10.1039/D0TA09337H.
[37] L. Kong, H. Cui, S. Zhang, G. Zhang, J. Yang, X. Fan, Absorption frequency band switchable intelligent electromagnetic wave absorbing carbon composite by cobalt confined catalysis, *Journal of Materials Science & Technology*, 2025, **211**, 203-211, doi: 10.1016/j.jmst.2024.03.085.
[38] L. Wang, Z. Ma, H. Qiu, Y. Zhang, Z. Yu, J. Gu, Significantly enhanced electromagnetic interference shielding performances of epoxy nanocomposites with long-range aligned lamellar structures, *Nano-Micro Letters*, 2022, **14**, 224, doi: 10.1007/s40820-022-00949-8.
[39] L. Wang, Z. Ma, Y. Zhang, L. Chen, D. Cao, J. Gu, Polymer-based EMI shielding composites with 3D conductive networks: a mini-review, *SusMat*, 2021, **1**, 413-431, doi: 10.1002/sus2.21.
[40] Y. Ning, X. Zeng, J. Huang, Z.-Y. Shen, Y. Gao, R. Che, Multifunctional electromagnetic responsive porous materials synthesized by freeze casting: principles, progress, and prospects, *Advanced Functional Materials*, 2025, **35**, 2414838, doi: 10.1002/adfm.202414838.
[41] A. Liu, H. Qiu, X. Lu, H. Guo, J. Hu, C. Liang, M. He, Z. Yu, Y. Zhang, J. Kong, J. Gu, Asymmetric structural MXene/PBO aerogels for high-performance electromagnetic interference shielding with ultra-low reflection, *Advanced Materials*, 2025, **37**, e2414085, doi: 10.1002/adma.202414085.
[42] Z. Zong, P. Ren, Z. Guo, J. Wang, Z. Chen, Y. Jin, F. Ren, Three-dimensional macroporous hybrid carbon aerogel with heterogeneous structure derived from MXene/cellulose aerogel for absorption-dominant electromagnetic interference shielding and excellent thermal insulation performance, *Journal of Colloid and Interface Science*, 2022, **619**, 96-105, doi: 10.1016/j.jcis.2022.03.136.
[43] Z. Ma, Z. Deng, X. Zhou, L. Li, C. Jiao, H. Ma, Z. Z. Yu, H.-B. Zhang, Multifunctional and magnetic MXene composite aerogels for electromagnetic interference shielding with low reflectivity, *Carbon*, 2023, **213**, 118260, doi: 10.1016/j.carbon.2023.118260.
[44] Z. Lei, D. Tian, X. Liu, J. Wei, K. Rajavel, T. Zhao, Y. Hu, P. Zhu, R. Sun, C. Wong, Electrically conductive gradient structure design of thermoplastic polyurethane composite foams for efficient electromagnetic interference shielding and ultra-low microwave reflectivity, *Chemical Engineering Journal*, 2021, **424**, 130365, doi: 10.1016/j.cej.2021.130365.
[45] L. Wang, J. Men, W. Ren, Z. Yang, Y. Gao, T. Gao, Y. Liu, X. Ji, Low-reflection electromagnetic interference shielding composite foams with asymmetric structure towards infrared camouflage and response switching, *Journal of Colloid and Interface Science*, 2025, **697**, 137941, doi: 10.1016/j.jcis.2025.137941.
[46] Z. Ma, Y. Zhang, R. Jiang, L. Shao, J. Cao, H. Guo, G. Zhang, Highly stretchable and room-temperature self-healing sheath-core structured composite fibers for ultrasensitive strain sensing and visual thermal management, *Composites Science and Technology*, 2024, **248**, 110460, doi: 10.1016/j.compscitech.2024.110460.
[47] Y. Wu, K. Huang, X. Weng, R. Wang, P. Du, J. Liu, S. Lin, K. Huang, H. Yang, M. Lei, PVB coating efficiently improves the high stability of EMI shielding fabric with Cu/Ni, *Advanced Composites and Hybrid Materials*, 2022, **5**, 71-82, doi: 10.1007/s42114-021-00401-2.
[48] X. Tang, Y. Lu, S. Li, M. Zhu, Z. Wang, Y. Li, Z. Hu, P. Zheng, Z. Wang, T. Liu, Hierarchical polyimide nonwoven fabric with ultralow-reflectivity electromagnetic interference shielding and high-temperature resistant infrared stealth performance, *Nano-Micro Letters*, 2024, **17**, 82, doi: 10.1007/s40820-024-01590-3.
[49] X. Zhao, X. Tang, Y. Qiao, S. Li, Z. Zhang, Y. Lu, M. Zhu, Z. Hu, L. Long, Z. Wang, T. Liu, Ultrathin polyimide-based composites with efficient low-reflectivity electromagnetic

shielding and infrared stealth performance, *Nano Research*, 2024, **17**, 6700-6712, doi: 10.1007/s12274-024-6650-1.
[50] Y. Xu, M. Hou, J. Wang, Porous gradient composite with dependable superhydrophobic protection for multifunctional electromagnetic interference shielding, *ACS Applied Materials & Interfaces*, 2024, **16**, 3978-3990, doi: 10.1021/acsami.3c15242.
[51] C. Wang, Z. Zhao, S. Zhou, L. Wang, X. Liu, R. Xue, Facile fabrication of densely packed ammoniated alumina/MXene/bacterial cellulose composite films for enhancing thermal conductivity and photothermal conversion performance, *Journal of Materials Science & Technology*, 2025, **213**, 162-173, doi: 10.1016/j.jmst.2024.06.024.
[52] S. Wang, Z. Sun, Y. Wang, T. Liang, B. Wang, C. Fan, Y. Chen, C. Liu, Q. Huang, Design of CuS composite carbon-based Ni Al-LDH multifunctional phase change composite with electromagnetic shielding performance and heat storage capacity, *Chemical Engineering Journal*, 2024, **491**, 151960, doi: 10.1016/j.cej.2024.151960.
[53] Y. Shang, Y. Ji, J. Dong, G. Yang, X. Zhang, F. Su, Y. Feng, C. Liu, Sandwiched cellulose nanofiber/boron nitride nanosheet/$Ti_3C_2T_x$ MXene composite film with high electromagnetic shielding and thermal conductivity yet insulation performance, *Composites Science and Technology*, 2021, **214**, 108974, doi: 10.1016/j.compscitech.2021.108974.
[54] Z. Guo, Y. Zhao, P. Luo, Z. Chen, P. Song, Y. Jin, L. Pei, F. Ren, P. Ren, Durable and sustainable $CoFe_2O_4$@MXene-silver nanowires/cellulose nanofibers composite films with controllable electric–magnetic gradient towards high-efficiency electromagnetic interference shielding and Joule heating capacity, *Chemical Engineering Journal*, 2024, **485**, 149691, doi: 10.1016/j.cej.2024.149691.
[55] J. Kim, Y. Choi, H. Jang, S. Jiong, X. Chen, B. Seo, W. Choi, Thermo-chemo-mechanically robust, multifunctional MXene/PVA/PAA-hanji textile with energy harvesting, EMI shielding, flame-retardant, and joule heating capabilities, *Advanced Materials*, 2024, **36**, 2411248, doi: 10.1002/adma.202411248.
[56] M. Ma, W. Tao, X. Liao, S. Chen, Y. Shi, H. He, X. Wang, Cellulose nanofiber/MXene/FeCo composites with gradient structure for highly absorbed electromagnetic interference shielding, *Chemical Engineering Journal*, 2023, **452**, 139471, doi: 10.1016/j.cej.2022.139471.
[57] J. Li, X. Zhang, Y. Ding, S. Zhao, Z. Ma, H. Zhang, X. He, Multifunctional carbon fiber@NiCo/polyimide films with outstanding electromagnetic interference shielding performance, *Chemical Engineering Journal*, 2022, **427**, 131937, doi: 10.1016/j.cej.2021.131937.
[58] L. Wang, W. Ren, X. Hu, M. He, J. Men, H. Guo, Y. Zhang, X. Shi, H. Qiu, X. Ji, Biomass materials and their derivatives for electromagnetic interference shielding: a review, *Journal of Materials Science & Technology*, 2026, **243**, 28-44, doi: 10.1016/j.jmst.2025.04.019.
[59] Q. Lv, Z. Peng, H. Pei, X. Zhang, Y. Chen, H. Zhang, X. Zhu, S. Wu, 3D printing of periodic porous metamaterials for tunable electromagnetic shielding across broad frequencies, *Nano-Micro Letters*, 2024, **16**, 279, doi: 10.1007/s40820-024-01502-5.
[60] G. Zhang, H. Wang, W. Xie, S. Zhou, Z. Nie, G. Niwamanya, Z. Zhao, H. Duan, Advancements in 3D-printed architectures for electromagnetic interference shields, *Journal of Materials Chemistry A*, 2024, **12**, 5581-5605, doi: 10.1039/D3TA07181B.
[61] K. Abedi, S. Miri, L. Gregorash, K. Fayazbakhsh, Evaluation of electromagnetic shielding properties of high-performance continuous carbon fiber composites fabricated by robotic 3D printing, *Additive Manufacturing*, 2022, **54**, 102733, doi: 10.1016/j.addma.2022.102733.
[62] S. Ghaderi, H. Hosseini, S. A. Haddadi, M. Kamkar, M. Arjmand, 3D printing of solvent-treated PEDOT: PSS inks for electromagnetic interference shielding, *Journal of Materials Chemistry A*, 2023, **11**, 16027-16038, doi: 10.1039/D3TA01021J.
[63] T. Xue, Y. Yang, D. Yu, Q. Wali, Z. Wang, X. Cao, W. Fan, T. Liu, 3D printed integrated gradient-conductive MXene/CNT/polyimide aerogel frames for electromagnetic interference shielding with ultra-low reflection, *Nano-Micro Letters*, 2023, **15**, 45, doi: 10.1007/s40820-023-01017-5.
[64] X. Hou, X. Feng, K. Jiang, Y. Zheng, J. Liu, M. Wang, Enhancing electromagnetic shielding property and absorption coefficients *via* constructing electromagnetic rings in Janus composites, *Composites Science and Technology*, 2024, **257**, 110809, doi: 10.1016/j.compscitech.2024.110809.
[65] J. Zhang, L. Zeng, X. Liu, D. Zhang, A. Gao, B. Xue, Q. Zheng, Y. Feng, L. Xie, Lattice-filler dual-gradient and hierarchical porous architectures customized by multiple-nozzle 3D printing towards excellent absorption-dominant electromagnetic interference shielding, *Composites Science and Technology*, 2025, **262**, 111058, doi: 10.1016/j.compscitech.2025.111058.
[67] S. Shi, Y. Si, Y. Han, T. Wu, M. I. Iqbal, B. Fei, R. K. Y. Li, J. Hu, J. Qu, Recent progress in protective membranes fabricated *via* electrospinning: advanced materials, biomimetic structures, and functional applications, *Advanced Materials*, 2022, **34**, e2107938, doi: 10.1002/adma.202107938.
[66] L. Tang, M. Jia, M. He, Q. Liu, Y. Lin, Y. Yi, X. Liu, X. Liu, Y. Tang, J. Gu, Fabrication, applications, and prospects for poly(*p*-phenylene benzobisoxazole) nanofibers, *SusMat*, 2024, **4**, e245, doi: 10.1002/sus2.245.
[67] S. Shi, Y. Si, Y. Han, T. Wu, M. I. Iqbal, B. Fei, R. K. Y. Li, J. Hu, J. Qu, Recent progress in protective membranes fabricated *via* electrospinning: advanced materials, biomimetic structures, and functional applications, *Advanced Materials*, 2022, **34**, e2107938, doi: 10.1002/adma.202107938.
[68] S. Chanthee, C. Asavatesanupap, D. Sertphon, T. Nakkhong, N. Subjalearndee, M. Santikunaporn, Electrospinning with natural rubber and Ni doping for carbon dioxide adsorption and supercapacitor applications, *Engineered Science*, 2024, **27**, 975, doi: 10.30919/es975.
[69] L. A. Mercante, R. S. Andre, M. H. M. Facure, D. S. Correa, L. H. C. Mattoso, Recent progress in conductive electrospun materials for flexible electronics: Energy, sensing, and electromagnetic shielding applications, *Chemical Engineering Journal*, 2023, **465**, 142847, doi: 10.1016/j.cej.2023.142847.

[70] J. Lei, Z. Han, L. Xiang, D. Pan, H. Liu, C. Shen, The preparation of SiO_2/SWCNT@Ni composite film with sandwich structure and its excellent electromagnetic shielding and thermal insulation performances in extreme environment, *Advanced Composites and Hybrid Materials*, 2025, **8**, 204, doi: 10.1007/s42114-025-01235-y.
[71] M. Chen, J. Zhu, K. Zhang, H. Zhou, Y. Gao, J. Fan, R. Chen, H. Wang, Carbon nanofiber/polyaniline composite aerogel with excellent electromagnetic interference shielding, low thermal conductivity, and extremely low heat release, *Nano-Micro Letters*, 2024, **17**, 80, doi: 10.1007/s40820-024-01583-2.
[72] X. Tang, H. Gao, X. Zhao, K. Lai, S. Li, M. Zhu, Z. Wang, T. Liu, Gradient-structured polyimide nonwoven fabrics for intelligent adjustable low-reflection electromagnetic interference shielding, *Materials Today Nano*, 2025, **29**, 100586, doi: 10.1016/j.mtnano.2025.100586.
[73] D. Gao, S. Guo, Y. Zhou, B. Lyu, X. Li, P. Zhao, J. Ma, Absorption-dominant, low-reflection multifunctional electromagnetic shielding material derived from hydrolysate of waste leather scraps, *ACS Applied Materials & Interfaces*, 2022, **14**, 38077-38089, doi: 10.1021/acsami.2c10787.
[74] Y. Zhang, H. Wu, S. Guo, Sandwich-structured surface coating of a silver-decorated electrospun thermoplastic polyurethane fibrous film for excellent electromagnetic interference shielding with low reflectivity and favorable durability, *ACS Applied Materials & Interfaces*, 2022, **14**, 40351-40360, doi: 10.1021/acsami.2c11971.
[75] H. Liu, J. Dang, C. Lei, Z. Zhu, X. Li, H. Ding, N. Tian, C. You, Y. Yang, Modulating interface of Ni-embedded hollow porous $Ti_3C_2T_x$ MXene film toward efficient EMI shielding, *Small*, 2025, e2410937, doi: 10.1002/smll.202410937.
[76] L. Wang, H. Qiu, P. Song, Y. Zhang, Y. Lu, C. Liang, J. Kong, L. Chen, J. Gu, 3D $Ti_3C_2T_x$ MXene/C hybrid foam/epoxy nanocomposites with superior electromagnetic interference shielding performances and robust mechanical properties, *Composites Part A: Applied Science and Manufacturing*, 2019, **123**, 293-300, doi: 10.1016/j.compositesa.2019.05.030.
[77] L. Wang, X. Shi, J. Zhang, Y. Zhang, J. Gu, Lightweight and robust rGO/sugarcane derived hybrid carbon foams with outstanding EMI shielding performance, *Journal of Materials Science & Technology*, 2020, **52**, 119-126, doi: 10.1016/j.jmst.2020.03.029.
[78] W. Tao, M. Ma, X. Liao, W. Shao, S. Chen, Y. Shi, H. He, X. Wang, Cellulose nanofiber/MXene/mesoporous carbon hollow spheres composite films with porous structure for deceased reflected electromagnetic interference shielding, *Composites Communications*, 2023, **41**, 101647, doi: 10.1016/j.coco.2023.101647.
[79] S. Han, N. Li, Y. Song, L. Chen, C. Liu, M. Xi, X. Yu, Y. Qin, T. Xu, C. Ma, S. Zhang, Z. Wang, E-beam direct synthesis of macroscopic thick 3D porous graphene films, *Carbon*, 2021, **182**, 393-403, doi: 10.1016/j.carbon.2021.06.035.
[80] W. Huang, J. Liang, K. Chen, Y. Yu, Y. Zhu, J. Li, C. Pan, Y. Guo, S. Lan, R. Yao, *In-situ* formed silicon oxycarbide nanowires into porous SiC(rGO) PDCs enable balanced enhancement of robustness and thermal management, *Composites Part B: Engineering*, 2024, **287**, 111828, doi: 10.1016/j.compositesb.2024.111828.
[81] W. Chu, J. Li, J. Lin, W. Li, J. Xin, F. Liu, X. He, Z. Ma, Q. Zhao, Honeycomb-like Polyimide/Fe_3O_4@PPy foam for electromagnetic wave shielding with excellent absorption characteristics, *Composites Science and Technology*, 2024, **249**, 110489, doi: 10.1016/j.compscitech.2024.110489.
[82] L. Zhu, R. Mo, C.-G. Yin, W. Guo, J. Yu, J. Fan, Synergistically constructed electromagnetic network of magnetic particle-decorated carbon nanotubes and MXene for efficient electromagnetic shielding, *ACS Applied Materials & Interfaces*, 2022, **14**, 56120-56131, doi: 10.1021/acsami.2c17696.
[83] Y. Wang, Y. Zhong, J. Kang, B. Zhang, Z. Ma, Q. Zhao, J. Li, Multifunctional rigid polyimide foams with outstanding EMI shielding and wave absorption *via* densification strategy, *Journal of Materials Science & Technology*, 2025, **227**, 155-163, doi: 10.1016/j.jmst.2024.12.021.
[84] Y. Mao, Y. Sheng, Z. Fan, J. Yang, J. Liu, C. Tang, S. Fu, Atmospheric pressure dried discontinuous pore gradient structured CNF-based aerogel for ultra-low reflection, broadband, and super-high EMI shielding, *Advanced Functional Materials*, 2025, **35**, 2421492, doi: 10.1002/adfm.202421492.
[85] Z. Wei, Y. Cheng, Y. Zhan, Y. Meng, N. Pan, H. Xia, Construction of conductive–magnetic networks and porous structures for fabricating rubber-based green shielding materials, *Composites Communications*, 2024, **46**, 101849, doi: 10.1016/j.coco.2024.101849.
[86] K. Ghosh, S. S. Roy, P. K. Giri, Phosphorus-doped $Ti_3C_2T_x$ MXene/PEDOT: PSS aerogel-based electromagnetic interference shields with unique combination of high green index and shielding effectiveness, *Materials Today Advances*, 2025, **26**, 100576, doi: 10.1016/j.mtadv.2025.100576.
[87] H. Fu, Y. A. Bai, S. Duan, H. Zhou, W. Gong, Structure design of multi-layered ABS/CNTs composite foams for EMI shielding application with low reflection and high absorption characteristics, *Applied Surface Science*, 2023, **624**, 157168, doi: 10.1016/j.apsusc.2023.157168.
[88] J. Huang, Y. Wang, L. Yuan, C. Huang, J. Liao, C. Ji, X. Luo, Large-area and flexible plasmonic metasurface for laser–infrared compatible camouflage, *Laser & Photonics Reviews*, 2023, **17**, 2200616, doi: 10.1002/lpor.202200616.
[89] X. Chen, D. Lai, Facile construction of flexible multilayered graphene-based composite films for excellent electromagnetic interference shielding with ultralow-reflection, *Carbon*, 2023, **214**, 118375, doi: 10.1016/j.carbon.2023.118375.
[90] T. Mai, L. Chen, Q. Liu, Z. Guo, M. Ma, Zeolitic imidazolate frameworks derived magnetic nanocage/MXene/nanocellulose bilayer aerogels for low reflection electromagnetic interference shielding and light-to-heat conversion, *Advanced Functional Materials*, 2025, **35**, 2417947, doi: 10.1002/adfm.202417947.
[91] R. Cheng, C. Chu, R. Tang, Z. Huang, P. Xu, Y. Ding, Sandwich-structured polyacrylate composite films for electromagnetic interference shielding with low reflection characteristics, *Progress in Organic Coatings*, 2024, **187**, 108155,

doi: 10.1016/j.porgcoat.2023.108155.
[92] L. Xu, S. Wan, Y. Heng, S. Wang, J. Yang, Y. Dong, Y. Fu, Q. Ni, Double layered design for electromagnetic interference shielding with ultra-low reflection features: PDMS including carbon fibre on top and graphene on bottom, *Composites Science and Technology*, 2023, **231**, 109797, doi: 10.1016/j.compscitech.2022.109797.
[93] Y. Chang, R. Hao, Y. Yang, G. Zhao, Y. Liu, H. Duan, Progressive conductivity modular assembled fiber reinforced polymer composites for absorption dominated ultraefficient electromagnetic interference shielding, *Composites Part B: Engineering*, 2023, **260**, 110766, doi: 10.1016/j.compositesb.2023.110766.
[94] T. Chen, J. Cai, X. Cheng, S. Cui, D. Zhang, D. Gong, Bio-inspired flexible versatile textiles for excellent absorption-dominated electromagnetic interference shielding, thermal management, and strain sensing, *Chemical Engineering Journal*, 2023, **477**, 147116, doi: 10.1016/j.cej.2023.147116.
[95] B. Sun, S. Sun, Y. Guo, H.-Y. Mi, X. Jing, X. Jiang, B. Dong, C. Liu, C. Shen, Asymmetric magnetic-electric dual-functional composite foams for ultra-efficient electromagnetic interference shielding with unprecedented low reflection, *Composites Part A: Applied Science and Manufacturing*, 2023, **164**, 107301, doi: 10.1016/j.compositesa.2022.107301.
[96] L. Jia, X. Ding, J. Sun, X. Zhang, X. Tian, A controllable gradient structure of hydrophobic composite fabric constructed by silver nanowires and polyvinylidene fluoride microspheres for electromagnetic interference shielding with low reflection, *Composites Part A: Applied Science and Manufacturing*, 2022, **156**, 106884, doi: 10.1016/j.compositesa.2022.106884.
[97] J. Yang, Y. Chen, B. Wang, Y. Zhou, X. Chai, X. Yan, W. Han, C. Liu, P. Lin, Y. Xia, H. Zhang, X. Liao, Gradient structure silicone rubber composites for selective electromagnetic interference shielding enhancement and low reflection, *Composites Science and Technology*, 2022, **229**, 109688, doi: 10.1016/j.compscitech.2022.109688.
[98] J. Zhang, D. Zhu, S. Zhang, H. Cheng, S. Chen, R. Tang, Z. H. Hang, T. Zhang, X. Zhang, Z. Yang, Asymmetric electromagnetic shielding performance based on spatially controlled deposition of nickel nanoparticles on carbon nanotube sponge, *Carbon*, 2022, **194**, 290-296, doi: 10.1016/j.carbon.2022.04.012.
[99] J. Lei, Z. Han, L. Xiang, D. Pan, H. Liu, C. Shen, The preparation of SiO2/SWCNT@Ni composite film with sandwich structure and its excellent electromagnetic shielding and thermal insulation performances in extreme environment, *Advanced Composites and Hybrid Materials*, 2025, **8**, 204, doi: 10.1007/s42114-025-01235-y.
[100] J. Qian, H. Zhan, H. Mi, X. Li, W. Zhong, X. Wang, C. Liu, C. Shen, Asymmetric electrical-magnetic composite foams with oriented cells fabricated by supercritical CO_2 foaming and thermal stretching for efficient absorption dominated electromagnetic interference shielding, *Composites Part A: Applied Science and Manufacturing*, 2024, **186**, 108428, doi: 10.1016/j.compositesa.2024.108428.
[101] M. He, X. Lv, Z. Li, H. Li, W. Qian, S. Zhu, Y. Zhou, Y. Wang, X. Bu, Research on efficient electromagnetic shielding performance and modulation mechanism of aero/organo/hydrogels with gravity-induced asymmetric gradient structure, *Small*, 2024, **20**, e2403210, doi: 10.1002/smll.202403210.
[102] Y. Zhang, S. Yang, Q. Zhang, Z. Ma, Y. Guo, M. Shi, H. Wu, S. Guo, Constructing interconnected asymmetric conductive network in TPU fibrous film: Achieving low-reflection electromagnetic interference shielding and surperior thermal conductivity, *Carbon*, 2023, **206**, 37-44, doi: 10.1016/j.carbon.2023.01.043.
[103] J. Yao, J. Zhou, F. Yang, G. Peng, Y. Liu, Z. Yao, F. Wu, H. Zeng, Multi-functional and multi-scenario applications for MXene aerogels with synergistically enhanced asymmetric modules, *Nano Research*, 2024, **17**, 3359-3368, doi: 10.1007/s12274-023-6154-4.
[104] L. Ma, L. Wei, M. Hamidinejad, C. B. Park, Layered polymer composite foams for broadband ultra-low reflectance EMI shielding: a computationally guided fabrication approach, *Materials Horizons*, 2023, **10**, 4423-4437, doi: 10.1039/D3MH00632H.
[105] Y. Wang, M. He, J. Tang, L. Huang, X. Wang, J. Yu, Liquid metal-coated textile with P(AAm-co-AA) ionogel encapsulation to mitigate electromagnetic radiation pollution, *Advanced Materials Technologies*, 2024, **9**, 2400008, doi: 10.1002/admt.202400008.
[106] J. Feng, J. Wang, W. Liu, S. Fan, D. Guo, M. Tan, B. Li, K. Guo, S. Zhang, Highly stretchable liquid-metal/elastomeric foam based on a slidable double network for absorption-dominated electromagnetic interference shielding, *ACS Applied Polymer Materials*, 2024, **6**, 4103-4113, doi: 10.1021/acsapm.4c00200.
[107] H. Duan, H. Zhu, J. Gao, D. Yan, K. Dai, Y. Yang, G. Zhao, Y. Liu, Z. Li, Asymmetric conductive polymer composite foam for absorption dominated ultra-efficient electromagnetic interference shielding with extremely low reflection characteristics, *Journal of Materials Chemistry A*, 2020, **8**, 9146-9159, doi: 10.1039/D0TA01393E.
[108] H. Cheng, L. Xing, Y. Zuo, Y. Pan, M. Huang, A. Alhadhrami, M. M. Ibrahim, Z. M. El-Bahy, C. Liu, C. Shen, X. Liu, Constructing nickel chain/MXene networks in melamine foam towards phase change materials for thermal energy management and absorption-dominated electromagnetic interference shielding, *Advanced Composites and Hybrid Materials*, 2022, **5**, 755-765, doi: 10.1007/s42114-022-00487-2.

Publisher's Note: Engineered Science Publisher remains neutral with regard to jurisdictional claims in published maps and institutional affiliations.

Open Access
This article is licensed under a Creative Commons Attribution 4.0 International License, which permits the use, sharing, adaptation, distribution and reproduction in any medium or format, as long as appropriate credit to the original author(s)

and the source is given by providing a link to the Creative Commons license and changes need to be indicated if there are any. The images or other third-party material in this article are included in the article's Creative Commons license, unless indicated otherwise in a credit line to the material. If material is not included in the article's Creative Commons license and your intended use is not permitted by statutory regulation or exceeds the permitted use, you will need to obtain permission directly from the copyright holder. To view a copy of this license, visit http://creativecommons.org/ licenses/by/4.0/.

©The Author(s) 2025